



**Politecnico
di Torino**



**AALBORG
UNIVERSITY**

Department of Environment, Land, and Infrastructure Engineering (DIATI).

Department of Architecture, Design, and Media Technology.

Master's Degree Thesis

Mitigating the Urban Heat Island Effect by Enhancing Green Structures and Implementing Double Skin Facades in Urban Areas.

Case study: Via Della Consolata, Torino, Italy.

Supervisors:

Prof. Paolo Dabove

Prof. Seyyed Morteza Hosseini

Candidate:

Amir Dehghan Lotfabad

301571

A.Y. 2024/2025

Contents

Acknowledgments.....	4
Abstract	5
1. Introduction.....	8
1.1. Background.....	8
1.2. Examining the Factors Influencing UHI	8
1.3. Urban Heat Island Mitigation Scenarios and State-of-the-Art	10
1.4. Objectives and Contributions.....	12
2. Materials and Methods	14
2.1. Data Gathering.....	14
2.1.1. Satellite Data.....	14
2.1.2. Weather Data.....	15
2.2. Remote Sensing Technique to Retrieve SUHI	15
2.2.1. Top of Atmospheric Spectral Radiance.....	15
2.2.2. The Conversion of Radiance to At-Sensor Temperature	16
2.2.3. The Normalized Different Vegetation Index (NDVI) Method for Emissivity Correction	16
2.2.4. Calculation of the Proportion of Vegetation.....	16
2.2.5. Calculation of Land Surface Emissivity.....	16
2.2.6. Retrieving the Land Surface Temperature	16
2.2.7. Estimation of SUHI.....	17
2.3. Numerical Simulation to Retrieve Canopy Urban Heat Island Considering Urban Geometry Modeling and the Simulation Period	17
2.3.1. Urban Heat Island Modeling with the Urban Weather Generator	18
2.3.2. Mean Radiant Temperature Calculation.....	19
2.3.3. Mean Radiant Temperature Validation.....	20
2.3.4. Measuring Outdoor Thermal Comfort (UTCI).....	21
2.3.5. Modeling of Green Wall.....	22
2.4. Evaluating carbon emission intensity in energy system	23
3. Results	25
3.1. SUHI Detection and Site Selection.....	25
3.2. Impact of Green Walls on Outdoor Air Temperature for Current Condition and Future Projection	25
3.3. The Enhancement Effect of the Green Wall on Mean Radiant Temperature and Outdoor Comfort Under Current and Future Climate Projections (2050).....	28

3.4. Mitigation Effect of Green Walls in the Condition of Maximum Direct Normal Radiation	31
3.5. Impact of Green Walls on Carbon Emission Intensity in 2050	36
4. Discussion	38
5. Limitation.....	42
6. Conclusion	42
Note on Publication.....	43
Acknowledgments:.....	43
Abbreviations	44
Nomenclature.....	44
Appendix A	45
Appendix A.1	45
Appendix B.....	46
Appendix B.1.....	46
Sources of Figures.....	47
References	47

Figure 1. Drivers of urban heat islands and the scope of the study.....	12
Figure 2. Flowchart of the analysis of the SHUHI and site selection along with the simulation workflow.	14
Figure 3. Mean radiant temperature validation.....	21
Figure 4. (a) Land surface temperature (°C) and study area detection; (b) SUHI ranges and study area detection.....	26
Figure 5. Comparison of air temperature (°C) during current and future projection (2050) climate conditions.	27
Figure 6. Mean radiant temperature (T _{mrt}) °C spatial heat map before and after the installation of the green walls and the enhancement effect of green walls under current weather conditions. a) 12 th January; b) 29 th March; c) 29 th July; d) 15 th October.	29
Figure 7. Mean radiant temperature (T _{mrt}) °C spatial heat map before and after the installation of the green walls and the enhancement effect of the green walls for future projection (2050) weather conditions. a) 12 th January; b) 29 th March; c) 29 th July; d) 15 th October.	30
Figure 8. Number of hours of direct sunlight received in each simulation period.	32
Figure 9. Outdoor comfort (UTCI) spatial heat map before and after the installation of the green walls and the enhancement effect of the green walls under current weather conditions. a) 12 th January; b) 29 th March; c) 29 th July; d) 15 th October.....	33
Figure 10. Outdoor comfort (UTCI) spatial heat map before and after the installation of the green walls and the enhancement effect of the green walls for future projection (2050) weather conditions. a) 12 th January; b) 29 th March; c) 29 th July; d) 15 th October.....	34
Figure 11. Enhancement of mean radiant temperature (T _{mrt}) °C and outdoor comfort (UTCI) at 12:00 PM on 29 July when the direct solar radiation is maximum; (a) mean radiant temperature changes under current climate conditions; (b) outdoor comfort changes under current climate conditions; (c) mean radiant temperature changes under future projection (2050) climate conditions; (d) outdoor comfort changes under future projection (2050) climate conditions.	35
Table 1. Table of state-of-the-art.	11
Table 2. Landsat 9 image characteristics.....	15
Table 3. Parameters for land surface temperature calculation.	17
Table 4. Simulation time periods.	18
Table 5. Ladybug urban weather generator simulation settings.	18
Table 6. Mean radiant temperature validation. MBE: Mean Bias Error, CVRMSE: Cumulative Variation of Root Mean Squared Error.....	20
Table 7. UTCI stress categories and ranges.	22
Table 8. Air temperature variation (°C) after introducing a green wall for all the simulation periods under current and future projection climate conditions.	25
Table 9. Comparison of carbon emissions intensity (kg CO ₂ /m ²) between the base model without a green wall and the enhanced model after installing the green walls.	36

Acknowledgments

I would like to begin by expressing my heartfelt gratitude to my parents for their unwavering love, encouragement, and support throughout this journey. Their belief in my abilities has been a constant source of strength and inspiration.

I am deeply thankful to my supervisors, Professor Paolo Dabove and Professor Seyyed Morteza Hosseini, for their invaluable guidance, support, and mentorship. Their expertise, constructive feedback, and encouragement have been instrumental in shaping the direction and quality of my research.

I would also like to express my deep appreciation to my girlfriend, Narges, for her constant support, understanding, and motivation. Her companionship and patience have been a great source of comfort and strength throughout this process. I extend my appreciation to my colleagues and peers for their collaboration and insightful discussions, which have enriched my learning experience and contributed to the success of this work.

Lastly, I am grateful to the Department of Environment, Land, and Infrastructure Engineering at the Polytechnic University of Turin and Aalborg University for providing an intellectually stimulating environment and the resources necessary to pursue my research. This journey has been both challenging and rewarding, and I am profoundly thankful for the opportunities I have been given.

Abstract

Urban heat island (UHI) which is the effect of having higher air temperature in urban areas, is the result of urbanization and changing the surface properties, as during the daytime, buildings and structures would absorb more solar radiation and reflect less. Conversely, during nighttime they emit more longwave radiation, and these phenomena exacerbate the effects of climate change, leading to higher energy consumption and reduced outdoor thermal comfort in urban areas. This research investigates the potential of green facades (GFs)—specifically Green Walls (GWs)—to mitigate the UHI effect and enhance urban thermal comfort under both current and future climate projections (2050).

The primary research questions addressed in this study are: How do GWs affect thermal comfort in urban environments, particularly in terms of air temperature, mean radiant temperature (T_{mrt}), Universal Thermal Climate Index (UTCI) and their effect in reducing carbon emissions by decreasing buildings energy demand. Using remote sensing techniques to detect existing surface UHI along with employing numerical simulation methods, this study models the effects of GWs on urban microclimates. A case study was conducted in the urban area of Via della Consolata, Turin, Italy, where simulations, validated with onsite measurements, were run for typical weeks across different seasons and future climate projections (RCP8.5 - 2050).

Simulation results show that the evaporative cooling effect of GWs does not significantly reduce air temperatures and in some hours during the day we would experience even higher air temperatures, with a maximum reduction of 1.6 °C during winter in the 2050 compared to baseline conditions. Additionally, we would face reduction in average mean radiant temperatures and outdoor comfort in both current and future climate projections in all the simulation periods. For instance, on 29th July, the mean radiant temperature (T_{mrt}) decreased by 1.92 (°C) at noon, when the solar radiation is at its maximum under current climate conditions, and by 2.27 (°C) in 2050. Additionally, improvement in UTCI by 0.51 (°C) under current climate conditions and by 0.55 (°C) in the 2050, indicating a notable improvement in outdoor thermal comfort during summer. Carbon emission intensity analysis reveals that GWs reduce cooling demand in summer, resulting in a decrease in overall carbon emission intensity from 0.100 [kg CO₂/m²] to 0.069 [kg CO₂/m²]. However, a slight increase in heating demand during the cold months led to an increase in carbon emission intensity from 0.527 [kg CO₂/m²] to 0.549 [kg CO₂/m²] in 12th January and 0.022 [kg CO₂/m²] to 0.032 [kg CO₂/m²] in 15th October. Despite this, the overall impact of GWs remains positive, contributing to more sustainable urban environments. These findings demonstrate that GWs offer an effective strategy for urban heat mitigation, improving both thermal comfort and energy efficiency and emphasizes the importance of integrating green infrastructure

into urban planning to address the challenges posed by climate change. This study contributes to the growing body of knowledge on sustainable urban solutions and provides a framework for incorporating GFs into future urban development strategies.

Keywords: Air Temperature; Climate Change; Green Wall; Mean Radiant Temperature; Urban Heat Island.



Introduction



1. Introduction

1.1. Background

In today's world, over half of the world's population (54 percent) lives in urban areas. The coming decades will bring further profound changes to the size and spatial distribution of the global population. The world's population in 2050 is projected to be 66 percent urban dwellers, with the global urban population projected to grow by 2.5 billion urban dwellers between 2014 and 2050 [1]. Urbanization can cause problems for city inhabitants. One of the more prominent problems is the UHI effect of the urban canopy layer, which can also increase energy consumption [2]. The UHI effect is responsible for having higher air and surface temperature [3]. On a sunny day, solar irradiation will heat up the surfaces during the day, while at night, the temperature in the environment will be lower, and the surfaces will exchange the absorbed heat with their colder surroundings. The surface temperature is the main parameter affecting the mean radiant temperature (T_{mrt}) and consequently the universal thermal climate index (UTCI), alongside relative humidity and wind speed. Understanding the factors influencing the UHI effect is crucial for better use of urban heat reduction strategies and solutions. The most utilized research methods in this area of research were numerical model simulation, followed by mobile or stationary ground-based measurements and remote sensing. While satellite-based observations focus on surface temperature on a mesoscale, numerical simulations and field measurements provide further environmental parameters that allow for human thermal comfort analysis at the pedestrian level and consider the air temperature instead of the surface temperature, which is essential to predict the effect of heat events on human health and energy consumption [4–6]. It is also known that the diurnal profiles of surface urban heat islands (SUHIs) differ from those of canopy UHIs. Large SUHI generally occurs during the daytime, while large canopy UHI generally occurs at night, and therefore spatial assessment of canopy UHI through remote sensing techniques at a fine scale may introduce estimation error [7].

1.2. Examining the Factors Influencing UHI

The studies with statistical models such as stepwise multiple linear regression (SMLR), XGBoost, bivariate and multivariate analysis, and Pearson correlation analysis highlight the effects of urban morphology, building geometries, and surface properties on the UHI. Findings consistently demonstrate a strong correlation between urban morphology and UHI effects, particularly in densely built areas with high-rise structures. The UHI effect is influenced by several key morphological parameters, including building height, density, size, aspect ratio, sky view factor (SVF), area, and orientation [6,8]. Of these factors, orientation is unique in its effects on energy use intensity and thermal comfort [9,10]. Building height and

volume would increase nighttime SUHI as they store heat during the day and release it at night, and density increases daytime SUHI by elevating heat absorption and increasing heat retention in cities. Conversely, wider urban canyons could reduce SUHI by allowing better air circulation as wind speed reduces nighttime SUHI [11]. Findings show that the three main morphological parameters affecting UHI are SVF, street length (SL), and pervious surface fraction. Two main parameters of the increase in the total length of the streets in the site and the decrease in the SVF, which has a negative correlation with the ratio of mean building height to mean street width in the sample site (H/W), would exacerbate the SUHI [7]. SVF ranges from 0 to a maximum of 1, which is completely open to the sky and is defined as the percentage of free sky at a specific location [12,13]. A moderate-to-high SVF can mitigate UHI, whereas extremely high SVF levels intensify it [14]. In a simulation study with Envi-met [15] of the effect of the built environment (H/W), urban greenery, and SVF on thermal comfort, a regression analysis showed that the effect of SVF on air temperature was smallest. In contrast, its effect on surface temperature and consequently T_{mrt} , as an important parameter influencing UTCI [16], is the largest. A 0.1 unit increase in SVF led to an increase of 1.6 °C and 2.4 °C in air temperature and 17.9 °C and 16.7 °C in T_{mrt} within N-S and E-W streets, respectively. It also proves the effect of the orientation of buildings, to be considered by designers for the future development of cities [17]. Ref. [18] concerned with the best urban morphology parameters on air temperature, solar radiation, wind speed, T_{mrt} , and Physiological Equivalent Temperature (PET) in three different sites in Nanjing, China, without considering anthropogenic heat emissions. They found that, in general, by increasing SVF, the air temperature would increase, and increasing building area is not the main cause of the increase in air temperature. However, the variation in T_{mrt} was greater than air temperature. The correlation between T_{mrt} and SVF is different between day and night, with a positive correlation in daytime and a negative correlation in nighttime. The T_{mrt} correlates positively with the distance between buildings, gaining solar radiation in the daytime, and has a negative correlation with building heights. They also found areas with lower SVF, lower distance between buildings, lower solar radiation, and consequently lower T_{mrt} and better PET [11]. Also mentioned other factors influencing SUHI and indicated that, instead of urban morphology, climate background has a weak correlation with SUHI, and the relationship between different climate zones and geographical locations is varied. Conversely, surface properties, such as enhanced vegetation index, are the most critical factor for mitigating daytime heat, since urbanization causes a significant reduction in greenness in urban areas, which reduces the evapotranspiration capacity within the city and subsequently enhances SUHI intensities.

1.3. Urban Heat Island Mitigation Scenarios and State-of-the-Art

One UHI mitigation strategy for existing urban context without configuration in the urban morphology and orientation is the modification and incorporation of sustainable building materials into the built environment by changing the albedo of surfaces such as pavements and facades with high thermal effects materials and painting materials to be bright and reflective in the summer [19]. However, Ref. [20] gave suggestions that changing albedo solely would not improve thermal comfort enough in extreme events and recommended using additional strategies such as shading and evaporative cooling, especially in areas with low aspect ratios. In this case, urban areas around the world are increasingly investing in networks of urban forests, gardens, and other forms of green infrastructure (Table 1) such as trees, which (irrespective of configuration) can reduce thermal sensation from “Very Hot” conditions to “Hot”, irrespective of the street canyon’s aspect ratio [21], green roofs, and vertical greenery systems (VGSs) for their benefits in improving a building’s thermal and acoustic insulation, reducing the urban heat island effect, increasing urban biodiversity, and improving air quality [22,23], and reducing cooling energy demand, which consequently reduces CO₂ emissions in summer months [24]. Climate change also presents opportunities to promote urban green infrastructure [25], which, as a climatic background, is considered one of the factors affecting UHI. It is important to understand how to intervene in particularly compact and dense urban structures where there is not enough space to implement nature-based solutions [26]. In densely urbanized areas, buildings’ surfaces (i.e., façades and rooftops) can offer room for the installation of vegetation [27]. One of the well-known green initiatives implemented in dense urban environments is vertical greening due to its small footprint and ability to cover a large surface area as well as lower installation costs [3,28]. It has also been concluded that in a densely urbanized area characterized by high-rising buildings, green walls are more beneficial in mitigating UHI than extensive green roofs (EGRs), which have a negligible effect on urban warming. Using plants is more beneficial than other devices on facades, as the temperature of the leaves is lower than other materials. Around 60% of solar radiation absorbed by plants transforms into latent heat and sensible heat by evaporative cooling, provided by evapotranspiration from the plants and the substrate [29–31]. Consequently, it can reduce the fluctuations of surface temperature, air temperature, and relative humidity, alongside the amount of particulate matter on the walls, by reducing the risk of most common degradation mechanisms induced by salts and frost in historic building materials [3] such as the once in Italy. Furthermore, the study in Turin, Italy, shows that these mitigation strategies are more effective in mitigating summer UHI when installed in canyons parallel to the main wind direction than in perpendicular ones. It also shows that it is necessary to increase plant watering to promote the stomatal opening for adapting

to UHI during summer heat waves [27]. It must be mentioned that more than three hours of direct sunlight is necessary for the growth of vegetation [32].

Table 1. Table of state-of-the-art. cei: carbon emission intensity; AP: air pollutants; EC: energy consumption; HBvc: heat balance of the vegetation canopy; ILP: indoor lighting performance; LW: longwave radiation; PET: psychological equivalent temperature; PMV: predicted mean vote; RH: relative humidity; SW: shortwave radiation; Ta: air temperature; Tf: foliage temperature; Tmrt: mean radiant temperature; To: operative temperature; Ts: surface temperature; Twbgt: wet bulb globe temperature; UTCI: universal thermal climate index; Wd: wind direction; Ws: wind speed.

Scenario and/or Goals	Year	Climate	Insite Measured Parameters (Sensor Based)	Methodology	Results	CEI	Future
Study on albedo configurations for walls and floors: [20]							
• Low: <0.3	2022	Csa	Ta; RH; Ws; Tmrt	Validated simulation	Ta; Tmrt; PET; Ts	×	×
• Medium: 0.3–0.7							
• High: >0.7							
• Green roofs	2023	Zone C	The data that has been used is confidential	Validated simulation	EC; AP; Ta; Tmrt; LW	×	×
• Tree planting [33]							
Varying greenery coverage: [31]							
• Green roofs	2018	Af	Ta; RH; Ws	Validated simulation	Ta averaged	×	×
• Green façade							
Analyzing two VGSs: [34]							
• With soil	2023	Dwa	Ta; Ts; Tmrt; RH; Ws	Experimental study	SW; LW; Tmrt; Ts	×	×
• With plant, soil (albedo 0.43), and high-albedo walls (0.78) positioned 0.4 m							
Vegetated green façade on reduced-scale buildings [35]							
	2017	Cfb	Ts Inside; Ta Inside	Experimental study	Ta; Ta Inside; Ts Inside; To	×	×
Two VGSs technologies: [36]							
• Green Walls (GWs)	2025	Csa	Ta; RH; Ws; Wd; SW; LW; Ts	Validated simulation	Tmrt; PET; UTCI	×	×
• Vertical Forest							
Configurations of:							
• Living walls (LWs)	2023	Cfa	Ta; RH; Wd; Ws	Validated simulation	Ta	×	×
• Green façades		Csa					
• EGRs							
Considering wind direction, scale, and orientations [27]							
Thermal impact of urban green systems on UHI [37]:							
• Trees	2024	Cfb	Not specified	Validated simulation	RH; Ts; Ta; Tmrt; PET	×	✓
• Living façades							
• High albedo pavements							
Thermal performance of 4 parametric green façade systems [38]							
	2024	BSk	Not specified	Validated simulation	EC; ILP	✓	×
Effect of GWs on urban microclimate [39]							
	2019	BWh	Ta; Wd; Ws; RH	Validated simulation	Ta; Ta Inside; PMV; RH	×	×
Thermal balance of vegetation canopy [29]							
	2019	Cfa	SW; LW; Tf; Ta; Ts; Ws; RH	Experimental Study	LW; SW; Ta; Ws; HBvc; Ts; EC; To; Twbgt	×	×

1.4. Objectives and Contributions

From the literature, it has been concluded that urban morphology, climate background, and surface properties are the main factors amplifying the UHI effect (Figure 1), leading to increased air and surface temperatures in cities. Green facades and green roofs have been widely studied for their cooling benefits, including impacts on air temperature, T_{mrt} , outdoor comfort, and energy efficiency, particularly during summer and heat waves, as well as in winter conditions. They conclude that vertical greenery systems have better cooling efficiency compared to horizontal surfaces such as green roofs. However, analyses of energy efficiency and outdoor comfort are limited to small-scale assessments, focusing on a single block. Additionally, they did not consider the effect of climate change and failed to evaluate how greenery can mitigate carbon emission intensity.

To fill this gap, our study aims to evaluate the effect of green walls on air temperature, T_{mrt} , and outdoor thermal comfort, as well as its contribution to reducing the (cei) of the Heating, Ventilation, and Air Conditioning (HVAC) systems under current and future climate projections. The study is conducted on the scale of a few blocks, considering all the outdoor walls are covered entirely by green walls.



Figure 1. Drivers of urban heat islands and the scope of the study.



Materials & Methods



2. Materials and Methods

The methodology of this study comprises two sections, as illustrated in Figure 2. The initial section is devoted to the analysis and detection of the urban area experiencing the intense SUHI effect. This is followed by the selection of the study area through the utilization of remote sensing techniques. The subsequent section involves the evaluation and simulation of the mitigation scenario of green walls.

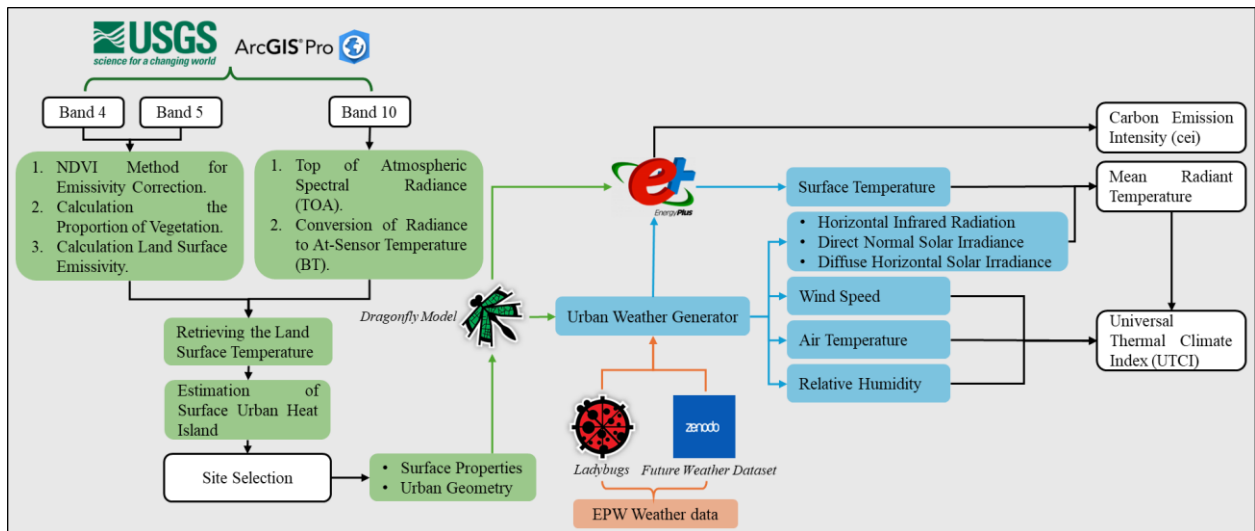


Figure 2. Flowchart of the analysis of the SUHI and site selection along with the simulation workflow.

2.1. Data Gathering

2.1.1. Satellite Data

The surface reflectance and emittance records of the Landsat-9 satellite were utilized in this study. The three Landsat-9 bands employed in this investigation were Band 4, Band 5, and Band 10 (Table 2). It is noteworthy that Band 4, which operates within the visible spectrum, possesses extremely short wavelengths. In contrast, the remaining bands function in regions of the spectrum that are imperceptible to the human eye. Band 5, which is sensitive to near-infrared (NIR) light, was particularly insightful. This region, which is reflected at maximum by healthy plants, which are the highest natural reflectors, up to 70%, can be used for the study of ecology. Band 10 operates within the thermal infrared (TIR) spectrum, detecting emitted thermal radiation. In contrast to the measurement of air temperature by a meteorological weather station, Band 10 reports the surface temperature, which is typically significantly hotter due to the ground's greater capacity for heat absorption and retention. The Landsat-9 satellite image and associated data were retrieved on 11 July 2023 [40]. The date was selected due to its representation of both the most recent and the oldest data, which predominantly covers the Turin municipality area with minimal cloud cover.

Table 2. Landsat 9 image characteristics.

Data Type	Time	Cloud Cover	Band Number	Resolution
Landsat 9 satellite imagery "OLI_TIRS"	11 July 2023, 11:16:53.4756430Z	3.34%	Band 4—Red	30.00 (m)
			Band 5—Near-infrared (NIR)	30.00 (m)
			Band 10—Thermal infrared 1 (TIRS1)	30.00 (m)

2.1.2. Weather Data

Weather data for creating site weather conditions were retrieved from Ladybug Tools EPWmap with the hourly temporal resolution [41] and the site meteorological measurements data gathered from [42] with hourly temporal resolution. The future meteorological data of the year 2050, considering RCP 8.5, relies on dynamical downscaling, following the approach outlined by the IEA EBC Annex 80 [43]—Weather Data Task Force. The most advanced approaches and tools for producing future global projections and weather files are referenced [44].

2.2. Remote Sensing Technique to Retrieve SUHI

In recent years, due to an increasing number of extreme meteorological events potentially related to climate change, growing attention has been paid to the operational use of satellite remote sensing applied to emergency management applications. This increased focus can be attributed to the substantial and prompt availability of diverse remotely sensed data types, along with geospatial information collected in situ [45]. In this study, we employed remotely sensed data and techniques to detect the SUHI effect and select our study case.

In the initial phase of the study, the methodologies employed for the SUHI computational mapping process were delineated into seven discrete steps.

2.2.1. Top of Atmospheric Spectral Radiance

As demonstrated in Figure 2, the initial step entails the calculation of the Top of Atmospheric (TOA) $L(\lambda)$ spectral radiance utilizing Eq. (1) [46,47] with the Raster Calculator Tool incorporated within ArcGIS Pro.

$$\text{TOA}(L(\lambda)) = \text{ML} \times \text{Qcal} + \text{AL}. \quad (1)$$

TOA ($L(\lambda)$) stands for Total Spectral Radiance ($\text{Watts}/(\text{m}^2 * \text{srad} * \mu\text{m})$), ML stands for the band-specific Multiplicative Rescaling Factor, Qcal refers to Band 10 of Landsat 9, and AL stands for the Band-Specific Additive Rescaling Factor. The MTL file is the only way to obtain the values for ML, Qcal, and AL. AL can be found in the MTL file by searching for RADIANCE ADD BAND 10 = 0.10000, and ML can be found in the MTL file by searching for RADIANCE MULT BAND 10 = 3.8×10^{-4} . Finally, Qcal is obtained by selecting Band 10 of the Landsat 9 image.

2.2.2. The Conversion of Radiance to At-Sensor Temperature

Subsequent to determining the TOA, the subsequent step entails the conversion of spectral radiance to the Top of the Atmosphere Brightness Temperature (BT), as delineated in Eq. (2) [46,47]. This conversion is performed by utilizing the thermal constants K1 and K2, which are obtained from the MTL file document, and the Total Spectral Radiance ($L\lambda$), which is the result of the preceding step.

$$BT = \frac{K2}{\ln\left[\left(\frac{K1}{L\lambda}\right)+1\right]} - 273.15. \quad (2)$$

It can be demonstrated that K1 and K2 can be discovered by finding the values of CONSTANT BAND 10, which are 799.0284 and 1329.2405, respectively.

2.2.3. The Normalized Different Vegetation Index (NDVI) Method for Emissivity Correction

The subsequent stage in the procedure entails the employment of the NDVI method for emissivity correction, as delineated in Eq. (3) [46,47]. This method holds paramount importance, as it is instrumental in determining the proportion of vegetation (P_v) through its application in calculating the Land Surface Emissivity (ϵ), a variable that is inextricably linked to the P_v [46,47].

$$NDVI = \frac{NIR(\text{band } 5) - Red(\text{band } 4)}{NIR(\text{band } 5) + Red(\text{band } 4)}. \quad (3)$$

2.2.4. Calculation of the Proportion of Vegetation

Substituting the results of Eq. (3) into Eq. (4) [46,47] yields the proportion of vegetation (P_v).

$$P_v = \left(\frac{NDVI - NDVI_{\min}}{NDVI_{\max} - NDVI_{\min}} \right)^2. \quad (4)$$

2.2.5. Calculation of Land Surface Emissivity

Afterwards, the next step is to calculate the (ϵ) using Eq. (5) [46] with the value of 0.004 and the correction value of 0.986 from the MTL file.

$$\epsilon = 0.004 \times P_v + 0.986. \quad (5)$$

2.2.6. Retrieving the Land Surface Temperature

The final step prior to calculating the SUHI value was to compute the Land Surface Temperature (LST). Utilizing the BT value previously obtained from Eq. (2), the LST in degrees Celsius ($^{\circ}\text{C}$) can be calculated through the application of Eqs. (6) and (7) [46,47] and the input parameters delineated in Table 3.

$$LST = \frac{BT}{\left\{1 + \left[\left(\frac{\lambda BT}{\rho}\right) \ln \varepsilon\right]\right\}} \quad (6)$$

$$\rho = h \frac{c}{\sigma} = 1.438 \times 10^{-2} (\text{mK}) \quad (7)$$

Table 3. Parameters for land surface temperature calculation.

Parameters	Values
Emitted radiance (λ)	10.800 (nm)
Stefan–Boltzmann constant (σ)	$5.667 \times 10^{-8} (\text{W/m}^2\text{k}^4)$
Light velocity (c)	$2.998 \times 10^4 (\text{m/s})$
Planck constant (h)	$6.626 \times 10^{-34} (\text{J})$

2.2.7. Estimation of SUHI

The term SUHI has been frequently employed to denote the difference in surface temperature between urban and rural areas. This can also be defined by quantification to consider urban surfaces' local and regional climate change. The SUHI is calculated using the following Eq. (8) [48], where T is LST, T_m is LST mean, and T_{sd} is the standard deviation of LST.

$$SUHI = \frac{T - T_m}{T_{sd}} \quad (8)$$

2.3. Numerical Simulation to Retrieve Canopy Urban Heat Island Considering Urban Geometry Modeling and the Simulation Period

Accurate building footprints have significant implications for urban planning and infrastructure management [49]. The geometric model that served as the foundation for all simulations was developed using the Rhinoceros 8 modeler. The dragonfly model was created based on dragonfly buildings from footprint geometry (horizontal Rhino surfaces). The buildings were created with the extrusion from building footprints based on digital elevation models, which represent an approximation of the building massing [50]. In addition to the selection of the urban site, the decision was made to decrease the run time for the comfort analysis by employing short time periods of four days taken from typical weeks in the (stat) file in the weather file of the weather station in Turin-Caselle Airport [41] (Table 4). The time period from 8:00 to 18:00, when the majority of activities are conducted, was selected for the simulation [12,33,51,52].

Table 4. Simulation time periods.

Typical Weeks	Selected Data
Extreme Cold Week (12 January–18 January)	12 January
Typical Spring Week (29 March–4 April)	29 March
Extreme Hot Week (27 July–2 August)	29 July
Typical Autumn Week (13 October–19 October)	15 October

2.3.1. Urban Heat Island Modeling with the Urban Weather Generator

UHI was incorporated into the present study by morphing the TMY weather data of the weather station through the integration of the validated Urban Weather Generator (UWG). The UWG approximates the thermal conditions of a city and utilizes several key geometric and material variables, as outlined in Table 5. These parameters are then entered into a generic model of the urban canyon, after which energy balance calculations are performed. Ultimately, the UWG morphed a TMY file, thereby adjusting the air temperature and relative humidity to reflect the urban conditions. Additionally, it incorporated anthropogenic heat fluxes resulting from exfiltration and waste heat from building HVAC systems [53–55].

Table 5. Ladybug urban weather generator simulation settings.

Model Parameters and Buildings Construction Set	
Climate Zone	Koppen Classification [3]/Cfa
Building Vintage	Pre-1980
Construction Type	Mass
Program	Medium Office [50], Conditioned
Terrain Properties	
Albedo (Reflectivity)	0.25 [56]
Thickness	0.5 (m)
Conductivity (Typical of Asphalt)	1 (W/mK)
Volumetric Heat Capacity (Typical of Asphalt)	1.6E6 (J/m ³ K)
Traffic Parameters	
Maximum Sensible Anthropogenic Heat	20 (W/m ²)
Albedo	0.25 [57]
Fraction of the Absorbed Solar Energy by Trees	0.7
Fraction of the Absorbed Solar Energy by Grass	0.5
EPW Site Parameters	
Obstacles Height	0.01 (m)
Vegetation Coverage	0.9
Temperature Height	17
Wind Height	10
Boundary Layer Parameters	
Day Height	1000 (m)
Night Height	80 (m)
Inversion Height	150 (m)
Circulation Coefficient	1.2
Exchange Coefficient	0.2 [54]
Model Geometric Variables	

Average Height	15.7 (m)
Footprint Density	0.41
Facade to Site	1.4
Green Façade Characteristics	
Air Gap	0.05 (m) [27]
Plant Height	0.1 (m)
Leaf Area Index (LAI)	3 [27]
Substrate	0.05 (m)
Leaf Reflection	0.22
Leaf Emission	0.95
Soil Reflection	0.3
Soil Emission	0.9
Stomata Resistance	180 (s/m)
Soil Thickness	0.22 (m)
Soil Conductivity	0.35 (W/mK)
Soil Density	1100 (kg/m ³)
Soil-Specific Heat	1200 (J/kg K)

2.3.2. Mean Radiant Temperature Calculation

In this section of the research, the objective is to evaluate the impact of a canyon's geometry and surface characteristics, including ground and facade reflectivity and emissivity, on the Tmrt simulation and its spatial distribution. This analysis is conducted using the method outlined in the literature [52,53,56].

In the first step of calculating, base longwave radiation would be computed Eq. (9) [53,56].

$$\text{LW MRT} = \left[\sum_{i=1}^N F_i T_i^4 \right]^{1/4} - 273.15 \text{ } ^\circ\text{C} \quad (9)$$

We consider T_i to be equivalent to the surface temperature, as derived from the EnergyPlus simulation. F_i is defined as the view factor for each surface, calculated through the ray-tracing capabilities of the Rhino 3D modeling engine. The model also incorporates the sky temperature and longwave loss to the sky in Eq. (10) [53,56], utilizing the horizontal infrared radiation contained within the TMY data.

$$T_{\text{sky}} = \frac{L_a}{(\varepsilon_{\text{person}} \sigma)^{1/4}} \quad (10)$$

In the context of outdoor shortwave solar radiation, which is defined as the direct incidence of solar radiation upon individuals, the SolarCal model [58] of ASHRAE-55 is defined. The SolarCal model is based on the Effective Radiant Field (ERF), a metric of the net radiant energy flux to or from the human body, as defined by Eq. (11) [53,56]. ERF is employed to delineate the supplementary (positive or negative) long-wave radiation energy at the body surface when the surrounding surface

temperatures deviate from the air temperature. It is in (W/m²), where area refers to body surface area.

$$ERF_{\text{solar}} = (0.5 \cdot f_{\text{eff}} \cdot f_{\text{svv}} \cdot (I_{\text{diff}} \cdot I_{\text{th}} \cdot R_{\text{floor}}) + A_p \cdot f_{\text{bes}} \cdot I_{\text{dir}} \cdot AD) \cdot (a_{\text{sw}} \cdot a_{\text{lw}}) \quad (11)$$

This ERF is converted into a Tmrt delta using the following Eq. (12) [53,56]:

$$ERF = f_{\text{eff}} h_r (MRT - LW MRT) \quad (12)$$

2.3.3. Mean Radiant Temperature Validation

In order to statistically evaluate the acceptability of the simulation and output for measuring Tmrt, a comparison will be made between them and the site-measured sensor data with the characteristics provided in Table A1. The validation was analyzed using the Mean Bias Error (MBE) Eq. (13) and the Cumulative Variation of Root Mean Squared Error (CVRMSE) Eqs. (14) and (15), in accordance with the ASHRAE Guideline 14 [52,59].

$$MBE = \frac{\sum_{i=1}^{N_p} (M_i - S_i)}{\sum_{i=1}^{N_p} M_i} \quad (13)$$

$$CVRMSE = \frac{\sqrt{\sum_{i=1}^{N_p} (M_i - S_i)^2 / N_p}}{M_p} \quad (14)$$

$$(\overline{M_p} = \frac{\sum_{i=1}^{N_p} M_i}{N_p}) \quad (15)$$

According to the ASHRAE Guideline 14, the acceptable limits for calibration are delineated as follows. When analyzing hourly data, the results must be within $\pm 10\%$ MBE and $\leq 30\%$ CVRMSE. The Tmrt and validation results for the MBE and the CVRMSE, respectively, are provided in Table 6 and Figure 3.

Table 6. Mean radiant temperature validation. MBE: Mean Bias Error, CVRMSE: Cumulative Variation of Root Mean Squared Error.

Date	MBE	CVRMSE
12 January	-8.96%	22.12%
29 March	-8.35%	17.56%
15 October	-1.97%	20.15%
29 July	5.22%	14.98%

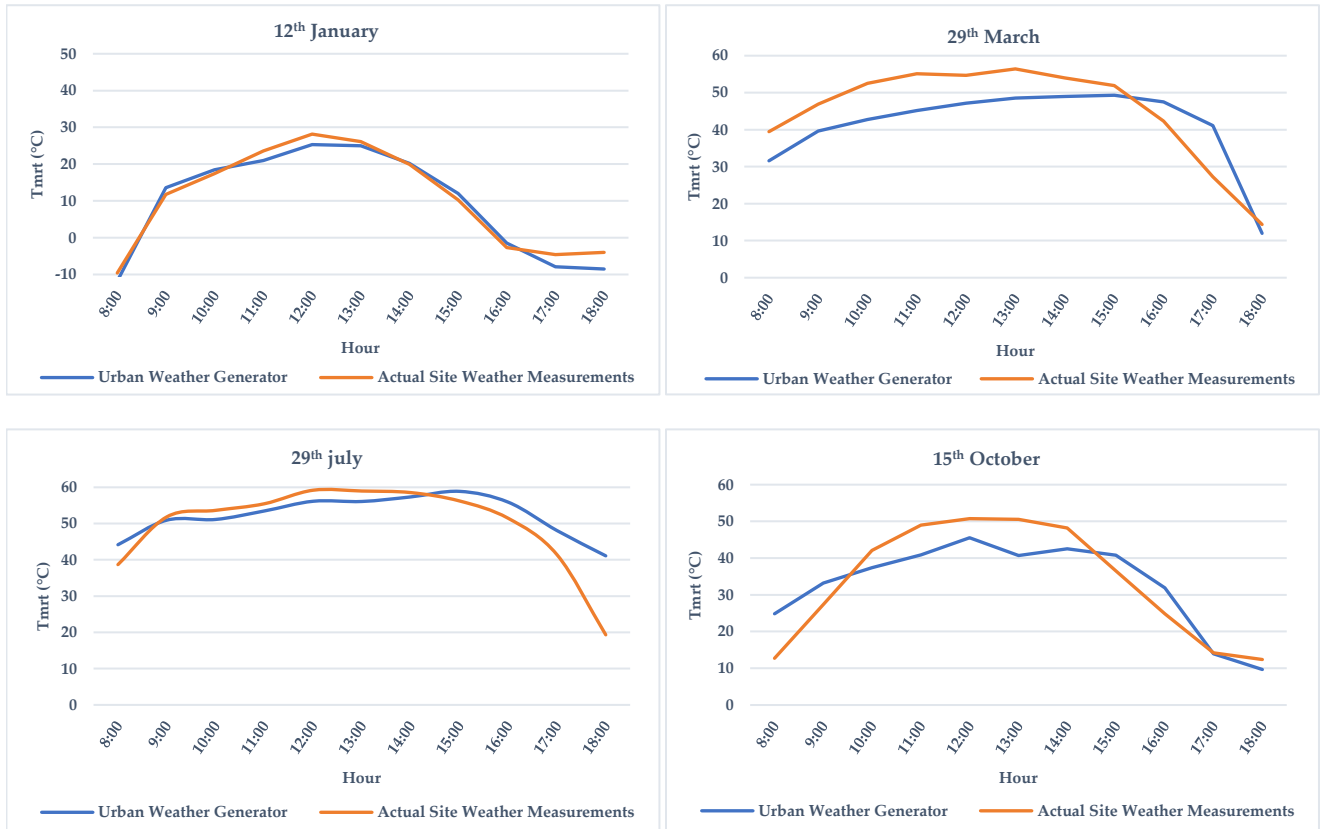


Figure 3. Mean radiant temperature validation.

2.3.4. Measuring Outdoor Thermal Comfort (UTCI)

UTCI, as an international standard for outdoor temperature sensation, is a thermal comfort model that quantifies how people perceive given weather conditions based on the range and stress category (Table 7) and is one of the most common temperatures used by meteorologists. While UTCI is designed to be valid in all climates and seasons, it operates under the assumption that human subjects are walking and that they naturally adapt their clothing to the outdoor temperature. For outdoor situations that do not fit these criteria, the Physiological Equivalent Temperature (PET) model is recommended. The calculation of the average UTCI over the specified time series, ranging from 8:00 to 18:00, necessitates the establishment of input parameters. These parameters, which are instrumental in determining the outdoor comfort levels, encompass wind speed data extracted from the designated weather file, mean air temperature measurements, relative humidity levels derived from the urban weather generator, and surface temperature values obtained from the URBANopt simulation conducted using EnergyPlus [60].

Table 7. UTCI stress categories and ranges.

Stress Category	Range °C
Extreme Cold Stress	$UTCI < -40$
Very Strong Cold Stress	$-40 \leq UTCI < -27$
Strong Cold Stress	$-27 \leq UTCI < -13$
Moderate Cold Stress	$-12 \leq UTCI < 0$
Slight Cold Stress	$0 \leq UTCI < 9$
No Thermal Stress	$9 \leq UTCI < 26$
Slight Heat Stress	$26 \leq UTCI < 28$
Moderate Heat Stress	$28 \leq UTCI < 32$
Strong Heat Stress	$32 \leq UTCI < 38$
Very Strong Heat Stress	$38 \leq UTCI < 46$
Extreme Heat Stress	$46 < UTCI$

2.3.5. Modeling of Green Wall

As stated in the article [61], which provides a categorization and comparison of various vertical greenery systems, including Green Barrier Systems, Green Coating Systems, and GWs, green walls have been found to be more effective in reducing outdoor surface temperatures and operative temperature. In this case, three categories have been proposed: the Mur Vegetal (MV), the Light Systems (LS), and the Heavy Systems (HS). The distinction between HS and LS lies in the soil thickness (less or greater than 15 cm, respectively).

In the present study, LS with the material properties delineated in Table 5 was employed. The GWs systems exhibit remarkable capacity to reduce the surface temperatures, which are also lower than those of the ambient air. Among the various systems, LS and HS have emerged as the most efficient ones in reducing the maximum temperature. However, the HS has a greater reduction in operative temperature in summer, while MV's effect on operative temperature in winter is greater. The thickness of the air gap and the type of soil are almost irrelevant in influencing the external surface temperatures, while the variation in LAI influences the external surface temperatures. Green walls (GWs) are characterized by the necessity of a higher degree of greater technical specialization in comparison to the other categories. The technology package (which includes the plants and the substrate) is supported by a subsystem and forms a gap with the walls, thereby exhibiting the characteristics of a ventilated façade. The ventilated cavity has been modeled as a separate thermal zone, and it has been conceptualized as a leaky building with a flow per exchange area of 0.0006 (m³/s per m² facade) and air changes per hour (ACH) of 3 [62,63].

2.4. Evaluating carbon emission intensity in energy system

The calculation can be utilized in the design of low- and net-zero-carbon buildings and districts. Carbon dioxide (CO₂) emissions per total energy supply refer to the quantity of kilograms of CO₂ released to produce a megawatt-hour (MWh) of energy. In this study, input emissions per total energy supply will be employed to calculate carbon intensity for both electricity and heating/cooling systems. The most recent carbon emissions of the Italian total energy supply for the year 2019 [64] were utilized as the reference value to compute the changes in energy consumption of our model and, consequently, the cei for the future projection 2050 emission report. In this study, the heating and cooling HVAC system was defined as a window AC with a baseboard gas boiler, and the service hot water system was defined as an electric water heater. The aggregated emission per total energy supply for the year 2019, with a value of 178.5 (kgCO₂/MWh), was considered in our analysis.



Results



3. Results

3.1. SUHI Detection and Site Selection

An analysis of surface temperature distribution across the Piedmont region of Italy revealed a significant thermal gradient, with temperatures ranging from 54 °C to 91 °C (Figure 4a). Statistical analysis indicated that nearly the entirety of the city would experience SUHI. Via della Consolata exhibited a very-high-intensity heat island region, which was selected as the study area. The Santuario della Consolata (7°40.7473753' E 45°4.6011994' N) is located at the center of this area (Figure 4b). The meteorological sensors mounted on the building record the following parameters: dry bulb temperature (°C), wind speed (m/s) and direction, relative humidity (%), atmospheric pressure, and irradiances (W/m²).

3.2. Impact of Green Walls on Outdoor Air Temperature for Current Condition and Future Projection

The installation of green walls exhibited intricate temporal variations in outdoor air temperature (Table 8). Under the prevailing climate conditions, the most substantial effects were observed during winter and spring, where temperature fluctuations ranged from a decrease of 0.3 °C to an increase of 1.3 °C on 12 January and from a reduction of 1.3 °C to an increase of 1.2 °C on 29 March. These variations exhibited robust diurnal and seasonal patterns, with the most pronounced cooling effects typically occurring until mid-afternoon hours, a phenomenon that persisted until 15 October. In contrast, summer conditions, as evidenced by measurements collected on 29 July, exhibited more modest and uniform modifications, ranging from 0 °C to +0.4 °C.

Table 8. Air temperature variation (°C) after introducing a green wall for all the simulation periods under current and future projection climate conditions.

Current weather condition											
Date	Hour										
	8:00	9:00	10:00	11:00	12:00	13:00	14:00	15:00	16:00	17:00	18:00
12 January	0.6	1.3	-0.2	-0.2	-0.2	-0.2	-0.3	-0.2	-0.3	-0.2	0.6
29 March	1.1	0.1	0	0	0	-0.1	-0.1	0	1.2	0.3	-1.3
29 July	0.2	0	0	0	0	0	0	0	0	0	0.4
15 October	0	0	0	0.1	0	0	-0.1	0	-0.4	-0.6	-0.6
Future projection 2050 (RCP8.5)											
Date	Hour										
	8:00	9:00	10:00	11:00	12:00	13:00	14:00	15:00	16:00	17:00	18:00
12 January	-0.3	-0.3	-0.3	-1.6	-0.3	-0.3	-0.2	-0.3	-0.3	-0.4	0.1
29 March	-0.2	-0.1	0	0	0	-0.1	0.3	0.2	0.3	0.7	0.5
29 July	0	0	0	0	0	0	0	-0.1	-0.1	-0.1	0.2
15 October	0	0.1	0	0	0	0	0	0	-0.1	-0.1	-0.1

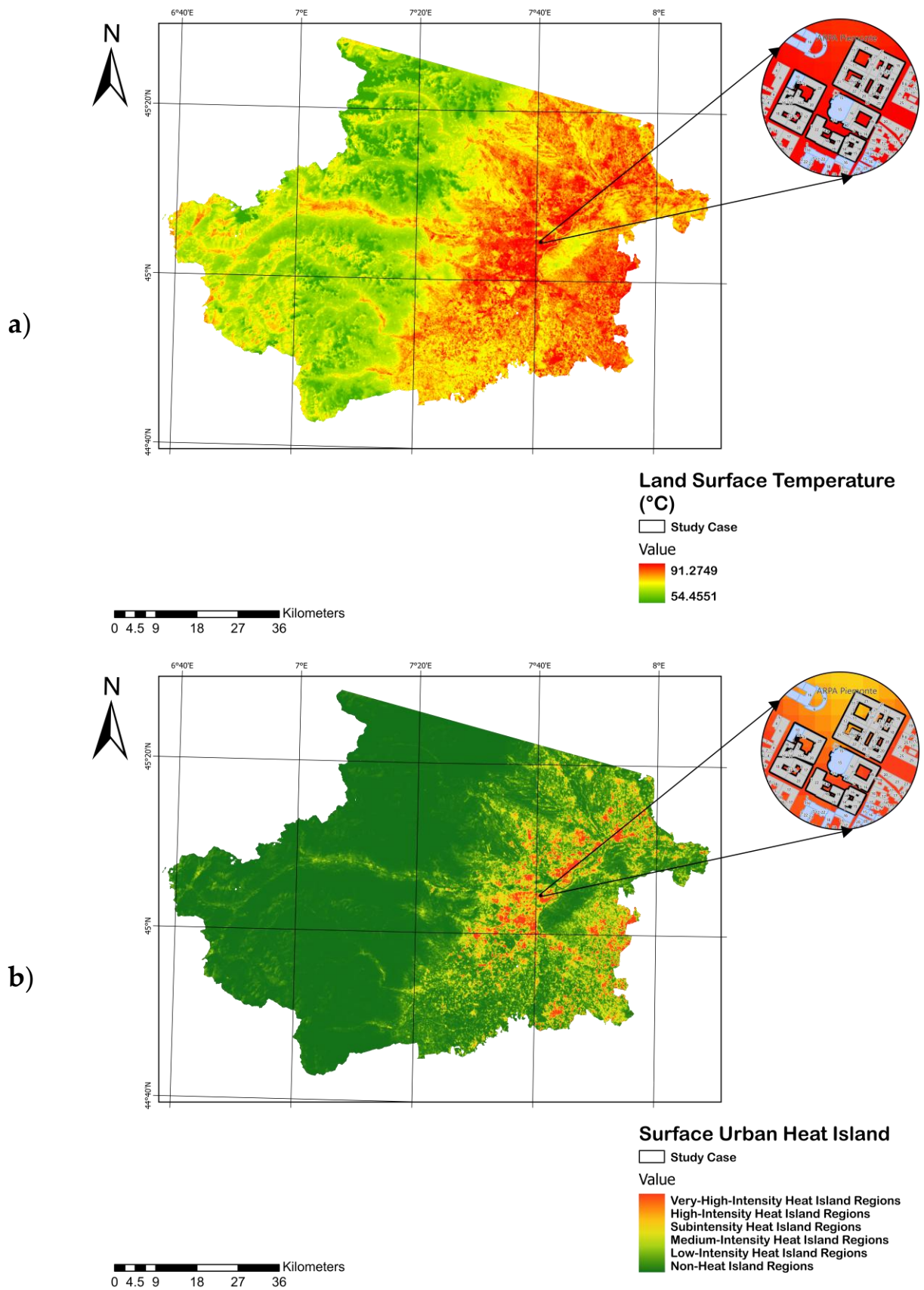


Figure 4. (a) Land surface temperature (°C) and study area detection; (b) SUHI ranges and study area detection.

In considering the broader context of urban heat island effects, future climate projections for 2050 are anticipated to exacerbate this phenomenon (Figure 5). However, the implementation of green walls could help counteract this trend by producing smaller temperature increases and more significant reductions, ranging from -1.6°C to 0.7°C , which highlight their potential as an effective mitigation strategy in the face of climate change. For instance, on 29 July, air temperatures under the current climate scenario exhibited some increases throughout the day. In contrast, future climate projections for 2050 demonstrated a consistent decline in temperature during the mid-afternoon hours. A similar trend was observed in winter. While early mornings—8:00 AM and 9:00 AM—under current conditions exhibited slight increases in air temperature, future projections indicated a notable decrease throughout the day, with more substantial reductions. The enhanced effectiveness under future climate scenarios suggests that green walls may become increasingly valuable as a climate adaptation strategy.

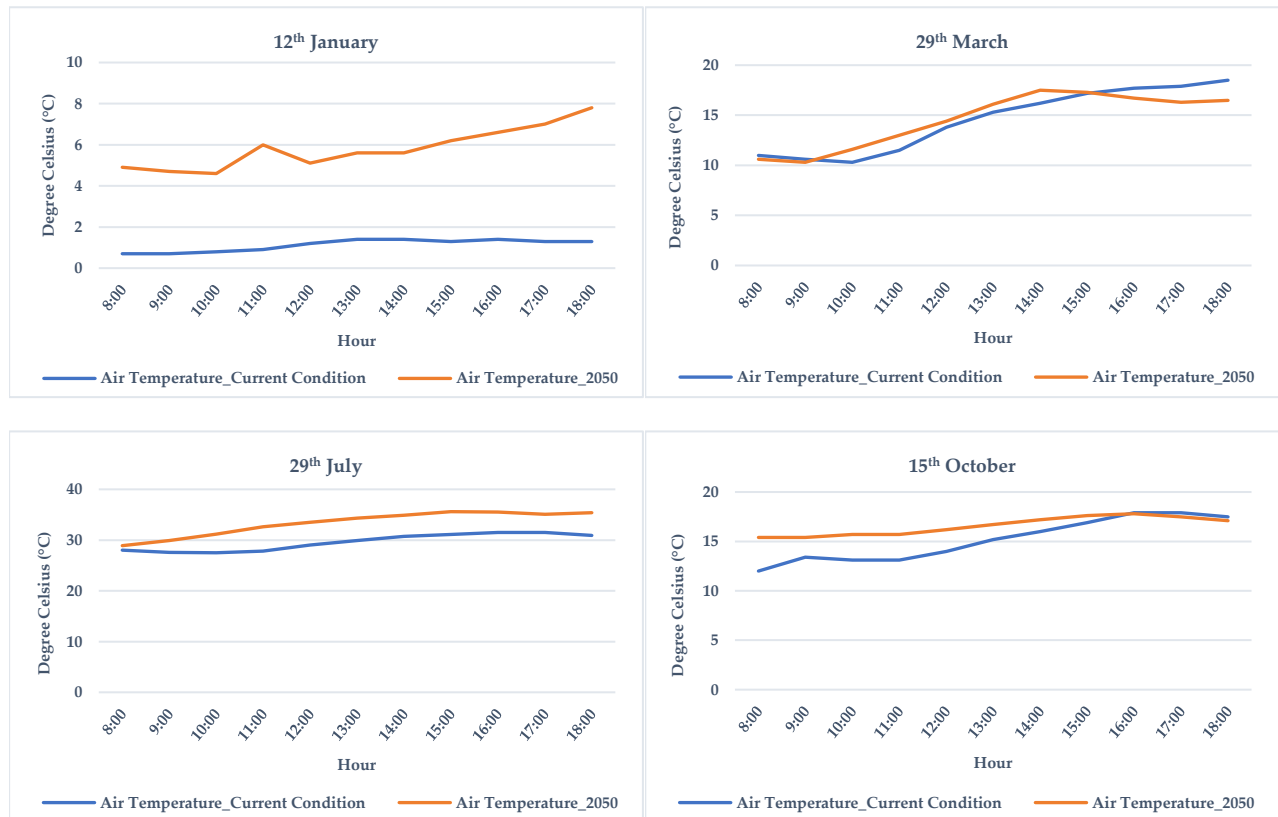


Figure 5. Comparison of air temperature ($^{\circ}\text{C}$) during current and future projection (2050) climate conditions.

3.3. The Enhancement Effect of the Green Wall on Mean Radiant Temperature and Outdoor Comfort Under Current and Future Climate Projections (2050)

An analysis of the cooling effect of the green wall on average Tmrt under current conditions and future climate projections is presented in Figures 6 and 7. Under current climate conditions, the green wall showed varying effects across different seasons. On 12 January, the results show an insignificant reducing effect with the values from -0.41°C to -0.22°C , showing a relatively modest effect with colder outdoor conditions, lower sun angle, and lower evapotranspiration efficiency. On 29 March the range of reductions was relatively higher, with the range from -0.64°C to -0.34°C . In contrast, on 29 July, the green wall exhibited the most substantial impact with the reduction, ranging from -1.10°C to -0.59°C , which is the consequence of having higher outdoor temperatures typical of summer, showing the effectiveness of the green wall in mitigating the UHI effect. Finally, cooler air temperatures on 15th October showed a smaller decrease in Tmrt from -1.07°C to -0.57°C .

In the case of the future projection 2050, in all the simulation periods we will experience higher outdoor air temperatures (Figure 5). In autumn and winter, instead of having warmer outdoor temperatures, the cooling effect of green walls was less impactful, with the mitigating from -0.34°C to -0.18°C on 15 October and -0.13°C to -0.07°C on 12 January. Considering having lower spatial Tmrt in 2050 because of lower radiation (Figure B1), and since solar radiation is a key driver of evapotranspiration, this condition results in less energy available to evaporate water from the soil and transpire water through the plants, thus having less cooling potential of green walls. Similarly, on 29th March, by considering having relatively higher air temperature and lower solar radiation (Figure B1), leading to lower spatial Tmrt, and better cooling performance with the averaged reduction from -1.25°C to -0.67°C . This could be the result of a greater temperature difference between air and surfaces resulting in better heat transfers.



Figure 6. Mean radiant temperature (Tmrt) °C spatial heat map before and after the installation of the green walls and the enhancement effect of green walls under current weather conditions. **a)** 12th January; **b)** 29th March; **c)** 29th July; **d)** 15th October.

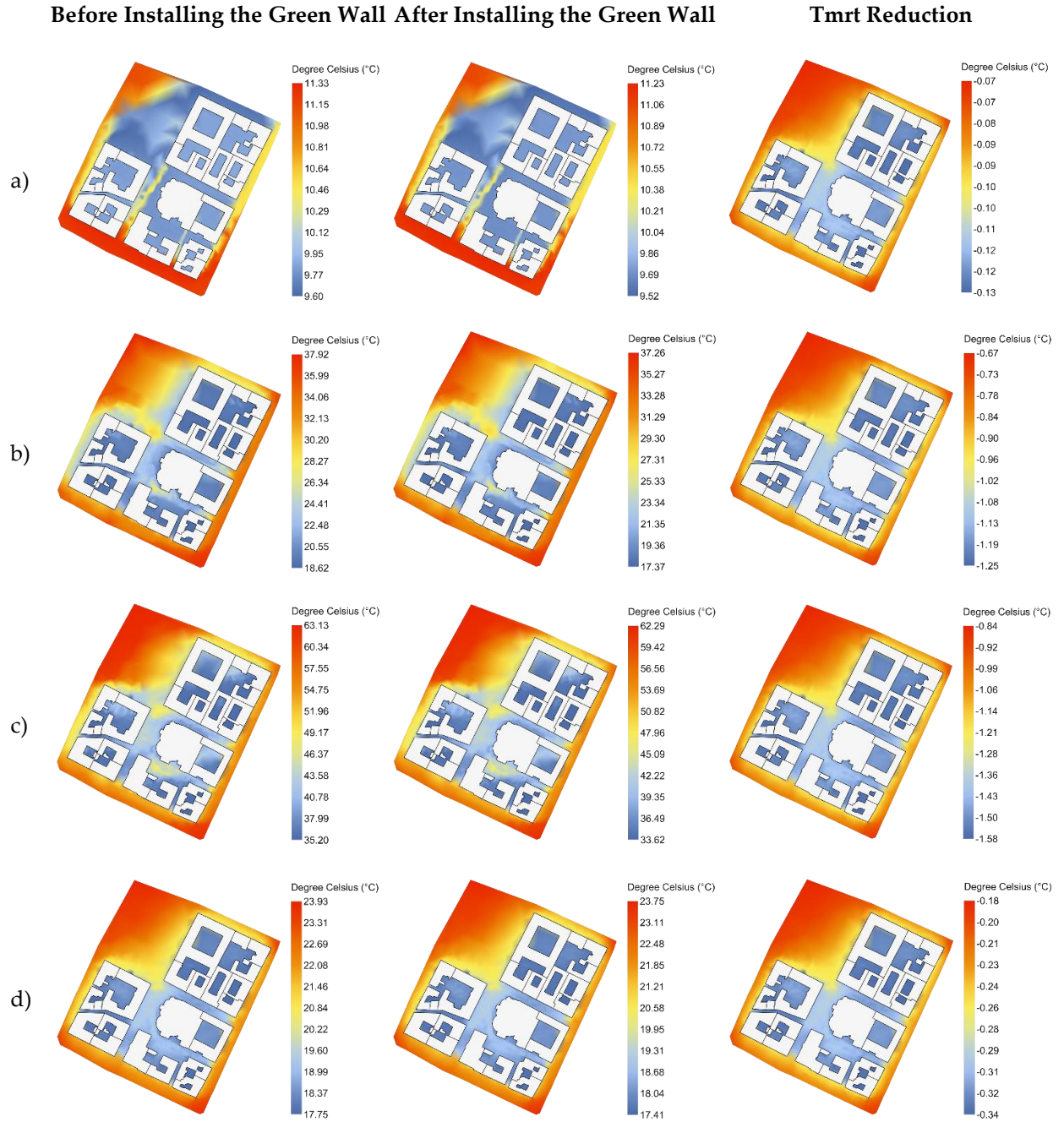


Figure 7. Mean radiant temperature (Tmrt) °C spatial heat map before and after the installation of the green walls and the enhancement effect of the green walls for future projection (2050) weather conditions. **a)** 12th January; **b)** 29th March; **c)** 29th July; **d)** 15th October.

On 29 July 2050, the relatively higher air temperature and solar radiation compared to current weather conditions cause an increase in average Tmrt and evapotranspiration by the leaves. In this case, the higher rate of evapotranspiration would result in better cooling performance of green walls with values from -1.58 °C to -0.84 °C. It is also worth noting that in all cases, the greatest reduction in Tmrt occurred in the canyons and courtyards with lower SVF and less direct sunlight exposure (Figure 8). In these areas, the main cause of higher Tmrt is longwave

radiation emitted from walls and pavements as they accumulate heat during the day and re-radiate it to the surrounding area, thus the heat has restricted the scattering paths. The shading effect of green walls would reduce the surface temperatures, hence decreasing longwave radiation emissions. Compared to open areas with better heat dissipation, this leads to a more pronounced cooling effect in low-SVF areas, where longwave radiation plays a dominant role. Additionally, in open areas, the T_{mrt} would decrease more in areas closer to the walls.

As presented in the literature, the most influential parameters affecting UTCI are T_{mrt} [16], air temperature, and relative humidity. It can be shown in (Figures 9) and 10 that the average UTCI experienced a reduction in all simulation periods after introducing the green wall to the model. The maximum reduction was recorded on 15 October by 0.44 °C and the minimum reduction on 12 January by 0.12 °C, under the current weather conditions.

Comparing the changes in outdoor comfort between future projection 2050 and current weather conditions, on 12 January and 29 July, we will experience worsening in outdoor comfort, which is the consequence of the greatest increase in air temperature (Figure 5). However, the enhancement effect of the green wall on thermal comfort would be maximum on 29 July by 0.40 °C.

In contrast, the change in air temperature was not significant on 29 March and 15 October. Furthermore, we will experience better outdoor comfort on 15 October with the least decreasing effect of the green wall and on 29 March, which corresponds to the lower T_{mrt} predicted in 2050.

3.4. Mitigation Effect of Green Walls in the Condition of Maximum Direct Normal Radiation

During the simulation period of the hottest week, climate change would amplify the T_{mrt} and UTCI. This is due to an increase in air temperature on 29th July at noon by 4.5 °C and maximum solar radiation with the values of 634 (Wh/m²) and 749 (Wh/m²) in current and future weather conditions, respectively. However, the cooling effect of the green wall will be more pronounced in 2050. The maximum reduction in T_{mrt} was recorded at 1.92 °C and 2.27 °C, and the maximum enhancement in outdoor comfort was recorded at 0.51 °C and 0.55 °C under current and future climate projections, respectively (Figure 11).

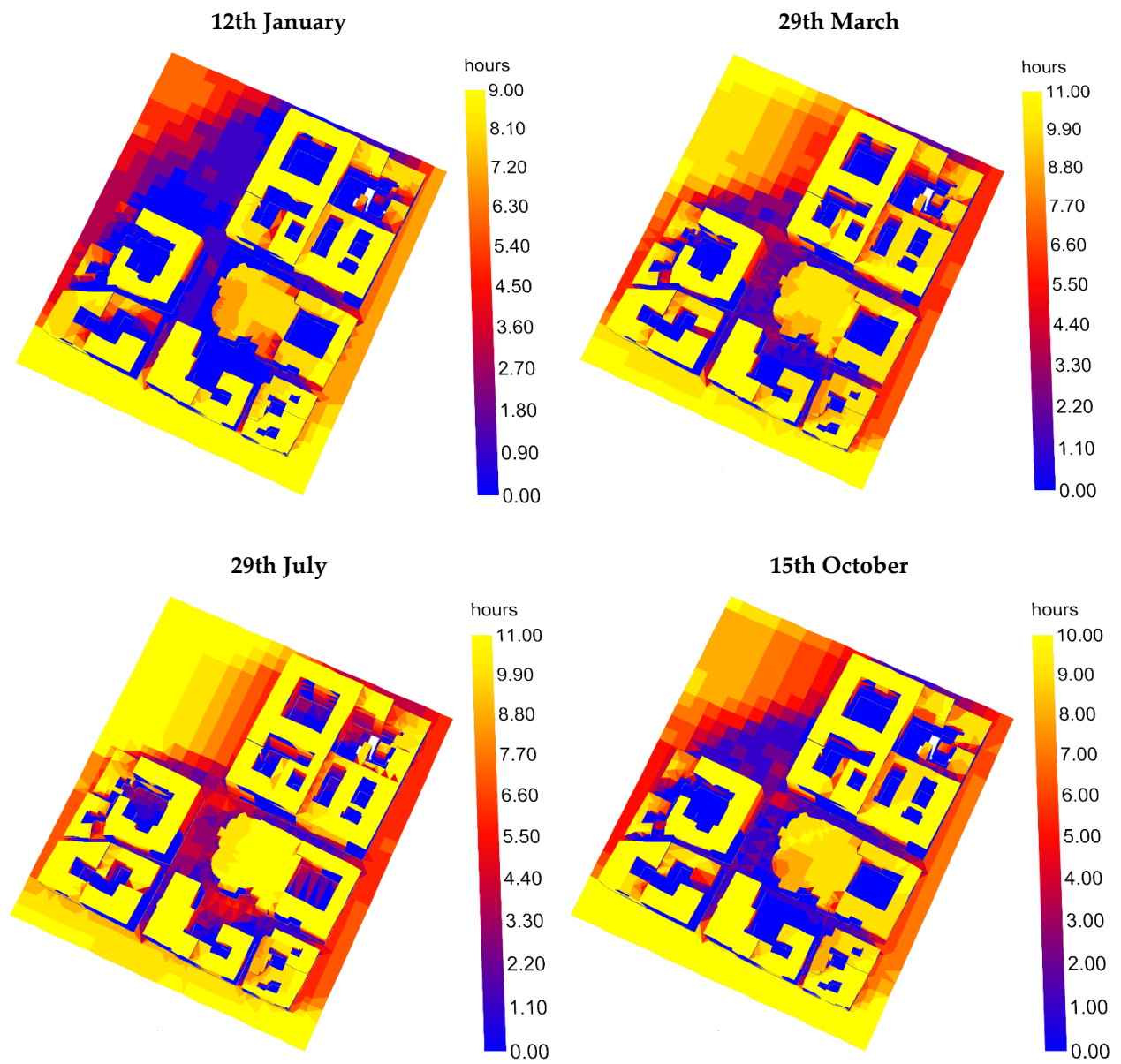


Figure 8. Number of hours of direct sunlight received in each simulation period.

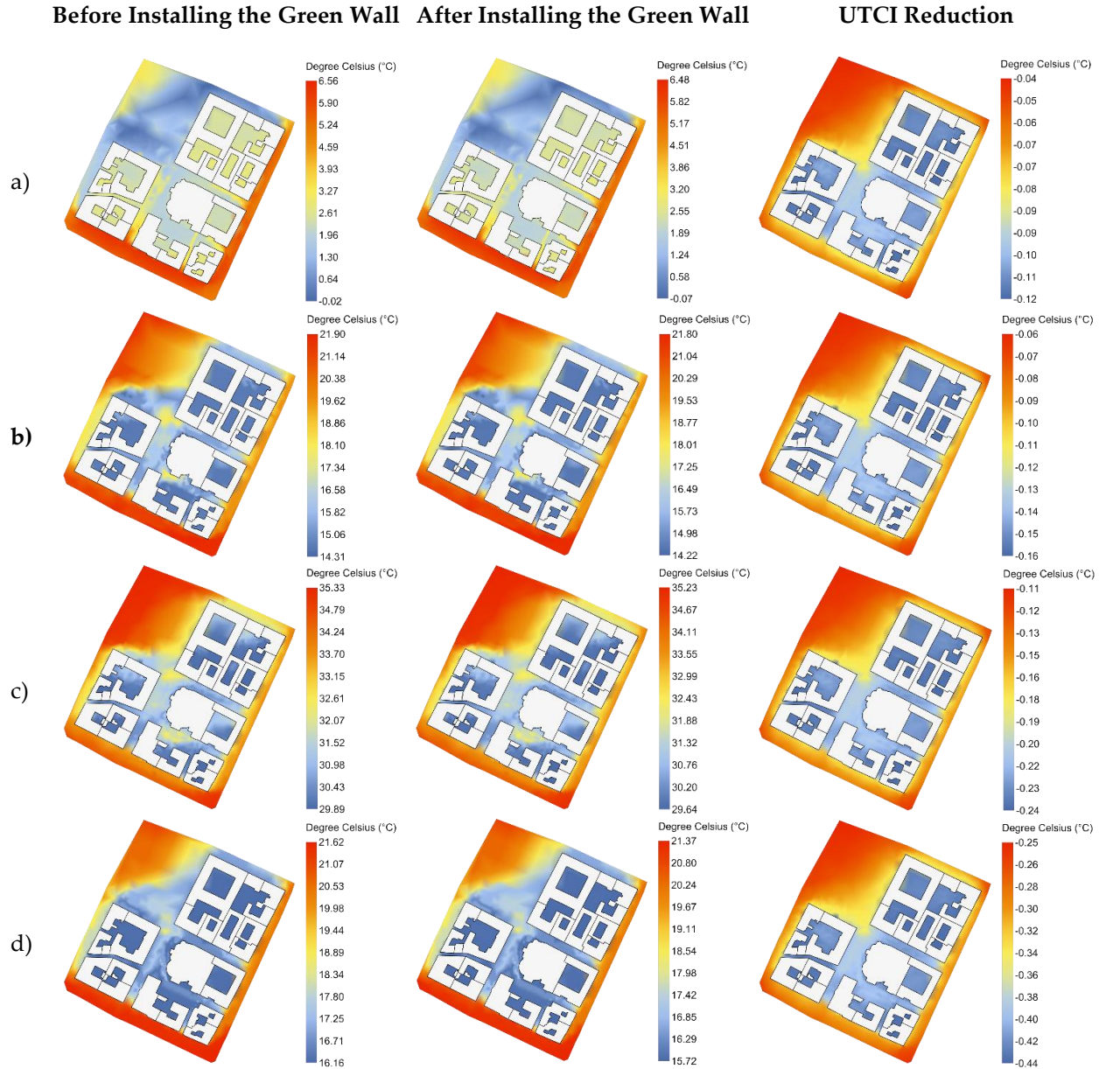


Figure 9. Outdoor comfort (UTCI) spatial heat map before and after the installation of the green walls and the enhancement effect of the green walls under current weather conditions. **a)** 12th January; **b)** 29th March; **c)** 29th July; **d)** 15th October.

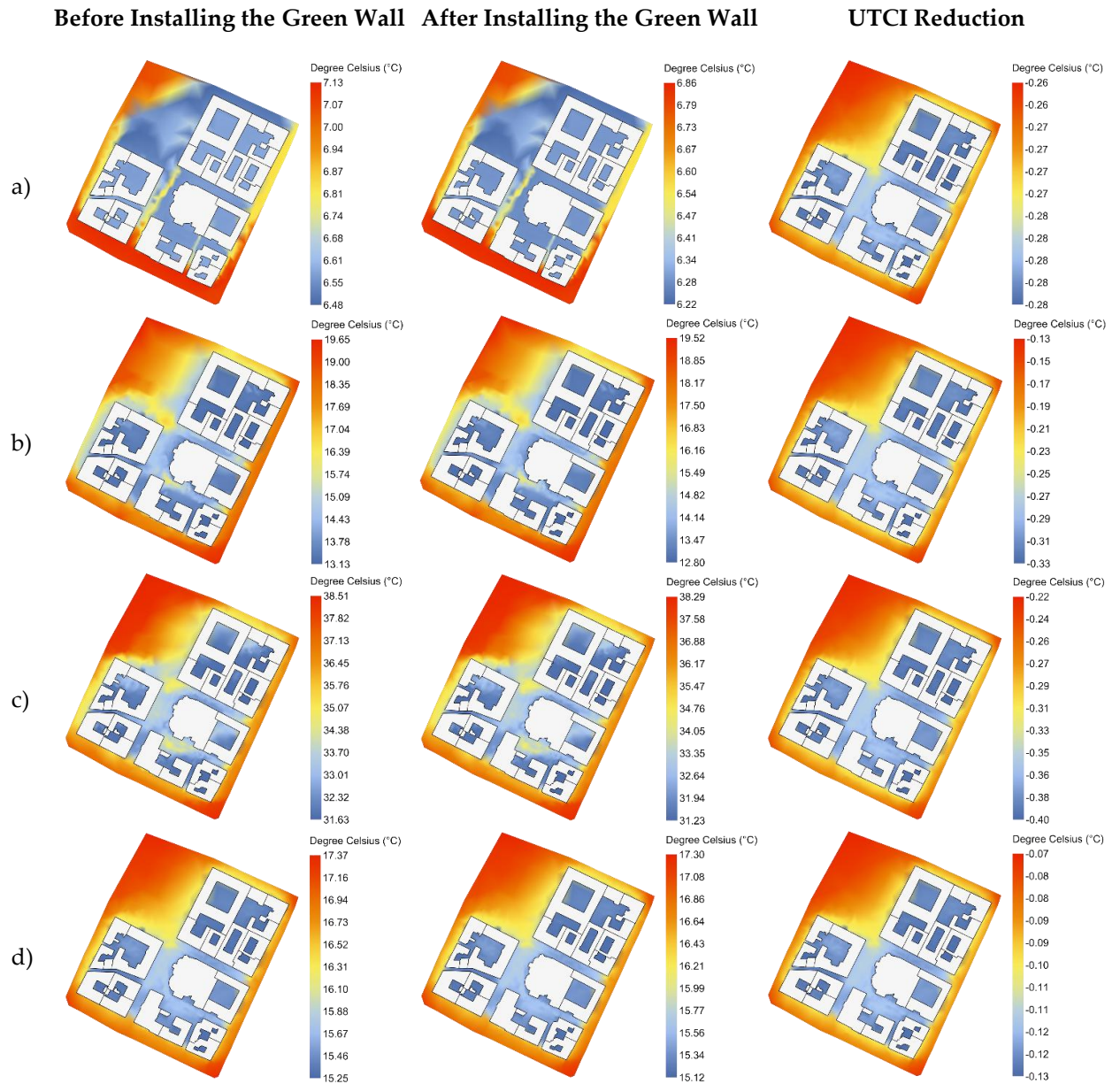


Figure 10. Outdoor comfort (UTCI) spatial heat map before and after the installation of the green walls and the enhancement effect of the green walls for future projection (2050) weather conditions. **a)** 12th January; **b)** 29th March; **c)** 29th July; **d)** 15th October.

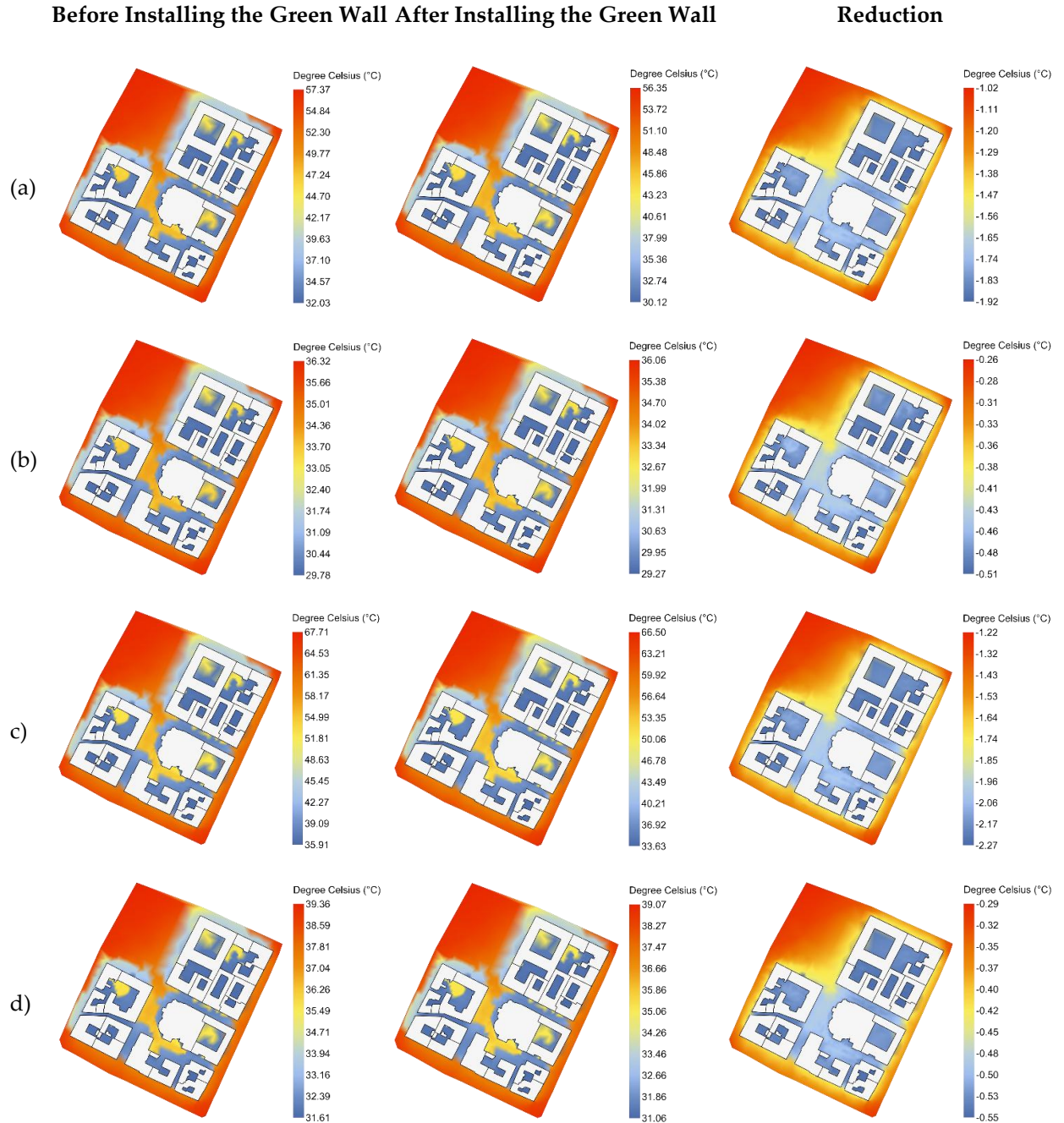


Figure 11. Enhancement of mean radiant temperature (T_{mrt}) °C and outdoor comfort (UTCI) at 12:00 PM on 29 July when the direct solar radiation is maximum; **(a)** mean radiant temperature changes under current climate conditions; **(b)** outdoor comfort changes under current climate conditions; **(c)** mean radiant temperature changes under future projection (2050) climate conditions; **(d)** outdoor comfort changes under future projection (2050) climate conditions.

3.5. Impact of Green Walls on Carbon Emission Intensity in 2050

On 12 January, there was an overall increase of 0.022 (kg CO₂/m²) in the (cei), primarily due to an increase in the heating demand from 0.495 (kg CO₂/m²) to 0.518 (kg CO₂/m²). Conversely, on 15th October, the total increase in (cei) amounted to 0.01 (kg CO₂/m²), with an increase in heating demand from 0.012 (kg CO₂/m²) to 0.022 (kg CO₂/m²). Conversely, on 29 July, a maximum reduction of 0.031 (kg CO₂/m²) was observed. This decline is attributed to a reduction in cooling demand from 0.085 (kg CO₂/m²) to 0.054 (kg CO₂/m²). The implementation of the green walls on 29 March led to a decline in overall cooling demand of 0.026 (kg CO₂/m²), reducing it from 0.028 (kg CO₂/m²) to 0.002 (kg CO₂/m²). Concurrently, there was an increase of 0.016 (kg CO₂/m²) from 0.025 (kg CO₂/m²) to 0.041 (kg CO₂/m²) in heating demand. As demonstrated in Table 9, the carbon emission results for each simulation day are based on the total gross floor area of 21,741 (m²). The installation of the green walls has been shown to result in a cooling effect, which would lead to an overall increase in energy demand during colder months and a reduction in energy demand during warmer months.

Table 9. Comparison of carbon emissions intensity (kg CO₂/m²) between the base model without a green wall and the enhanced model after installing the green walls.

Date	End Uses	Before Installing the Green Wall	After Installing the Green Wall
12 January	Heating	0.495	0.518
	Interior Lighting	0.011	0.011
	Electric Equipment	0.018	0.017
	Water Systems	0.003	0.003
	cei	0.527	0.549
29 March	Heating	0.025	0.041
	Cooling	0.028	0.002
	Interior Lighting	0.019	0.019
	Electric Equipment	0.031	0.031
	Water Systems	0.005	0.005
	cei	0.108	0.098
29 July	Cooling	0.085	0.054
	Interior Lighting	0.003	0.003
	Electric Equipment	0.010	0.010
	Water Systems	0.002	0.002
	cei	0.100	0.069
15 October	Heating	0.012	0.022
	Interior Lighting	0.001	0.001
	Electric Equipment	0.008	0.008
	Water Systems	0.001	0.001
	cooling	0	0
	cei	0.022	0.032



Discussion



4. Discussion

The implementation of VGSs in urban environments reveals complex and sometimes contradictory effects on microclimate parameters and building energy performance. This study's findings both challenge and confirm existing understanding of green wall performance in urban settings.

The extant literature suggests that the introduction of VGSs would result in positive cooling effects through transpiration and evaporative processes. Our results indicate minimal reductions in air temperature, and, in some cases, some similarities can be detected compared to several prominent studies in the literature. A distinguishing feature of our research is the examination of a more expansive urban area, encompassing complete facade coverage, in contrast to the smaller-scale studies and diverse typologies of vertical greenery systems and climate zones that are frequently focused on in the existing literature.

Air temperature changes, ranging from -1.6°C to 1.3°C , depending on the season and simulation period, show the insignificant cooling effect of green walls on outdoor air temperature and some exceptions when the heating effect occurred on several occasions [36], especially in summer. Similarly, [37] provided insignificant reduction in air temperature, ranging from -1.17°C to -0.09°C after the installation of LWs in different climate zones (Cfb). The cooling effect of green walls can be comprehended as well in a semi-arid climate zone (BWh) with double the thickness in the substrate. However, the range was much greater with a maximum reduction of 10°C [39]. However, the results are partly aligned with the previous study [27] being conducted in the same study area, with the difference between the typology of the VGSs, lower substrate thickness, and coverage area. This would provide additional information that, in the same area, even with different types of LWs, increasing the greenery coverage area would result in better cooling performance [31,55].

In addition to air temperature, the results also highlight reductions in T_{mrt} and outdoor thermal comfort indices [37]. Considering the effect of wall albedo configuration after introducing green walls as low-albedo surfaces with leaf and soil reflection values of 0.22 and 0.3, the findings showed better cooling effects on air temperature compared to the findings of [20]. Their study concluded that changing the albedo of the wall does not significantly improve air temperature and suggested evaporative cooling as a more effective strategy. In this context, the green walls, despite having low albedo, demonstrated enhanced cooling through the evaporative cooling effect provided by vegetation, aligning with their recommendations. Furthermore, the extant literature has explored the effect of surface albedo on localized T_{mrt} . Research findings indicate that modifying solely the albedo of vertical surfaces with inherently low albedo values frequently results in

deterioration of the T_{mrt} reduction effect. The findings indicate that medium albedo walls (0.4) would have a better mean delta T_{mrt} reduction of $-1.5\text{ }^{\circ}\text{C}$, which is superior to that of low albedo walls (0.1). The mean delta T_{mrt} reduction was found to be $-0.8\text{ }^{\circ}\text{C}$ [20], and in some cases, there was an increase in temperature, with values ranging from $1.8\text{ }^{\circ}\text{C}$ to $3.5\text{ }^{\circ}\text{C}$ during winter and from $2\text{ }^{\circ}\text{C}$ to $4\text{ }^{\circ}\text{C}$ during summer in all the climates under study [52]. However, our findings demonstrated that green walls, even with low albedo, would effectively improve T_{mrt} [20,52]. Our findings directly reflect the expected improvement in thermal comfort mentioned in the introduction, where green infrastructure is suggested to reduce the UTCI by mitigating heat exposure. The reduction in UTCI values indicates the effectiveness of green wall thermal properties in alleviating thermal stress as a mitigation strategy that can locally counteract the effects of climate change. The decrease in T_{mrt} and UTCI under current climate conditions during summer, particularly during the hours around noon, is also consistent with the literature [36], which suggests that green walls can lower T_{mrt} by blocking direct solar radiation and increasing local shading. UTCI values also showed similar improvement with the green walls in place.

Our findings are significantly consistent with theories about urban canyon effects on thermal performance. Studies like [14] identify SVF as a primary contributor to urban heat island intensity, suggesting that moderate-to-high SVF can mitigate UHI, whereas extremely high SVF levels intensify it, where in some studies the cooling effects of VGSs on air temperature were greater in central canyons [31]. Similarly, our results demonstrate that these areas show enhanced cooling benefits from green walls, with T_{mrt} reductions and outdoor comfort improvements greater than in open areas [16]. This challenges current urban design paradigms and suggests that VGSs might be particularly valuable in dense urban environments previously considered challenging for thermal management.

Results from [38] show almost a 29% reduction in annual carbon emissions can be expected. [33] Also concluded that greenery systems such as green roofs and trees would cause a reduction even in the energy performance of the buildings, which consequently results in the reduction in (cei). In our study, (cei) reduction ranges from 9% to 31% for spring and summer, although there was some increase in autumn and winter of 4% and 45%.

Our studies have shown that green walls have a significant impact on energy efficiency, especially in warm seasons. However, climate change may exacerbate or moderate these effects. Rising temperatures and the occurrence of heat waves in the future will double the importance of the cooling role of green walls, as this mitigation strategy can help reduce the urban heat island effect and increase thermal comfort. On the other hand, in cold seasons, climate change may cause changes in energy consumption patterns. A decrease in cold days or changes in the

intensity of winter colds can reduce the negative impact of green walls on energy consumption. For this reason, the design and implementation of greenery systems must be adapted to future climate conditions and possible temperature changes to increase energy efficiency and control carbon dioxide emissions.



Final Considerations



5. Limitation

In the context of outdoor comfort analysis, there exists a paucity of modeling tools that can predict microclimatic parameters, including air temperature and T_{mrt} . The predominant and widely utilized methods and software for calculating T_{mrt} are ENVI-met and Ladybug Tools. These tools are designed to calculate radiation components, including direct, diffuse, and reflected shortwave and longwave radiation from surfaces. Notably, both tools incorporate the calculation of longwave radiation from the sky. Both tools incorporate view factors, with Ladybug Tools utilizing ray-tracing and Envi-met employing Indexed View Sphere (IVS) methods. A distinguishing feature of both tools is their capacity to model radiation exchange between buildings, vegetation, and surface temperatures, which is a critical input parameter for T_{mrt} calculation. The primary distinction between the two tools lies in their approach to wind profiles. Envi-met utilizes a 3D computational fluid dynamics (CFD) model, a technique that has proven to be highly effective in simulating convective cooling or warming caused by wind. In contrast, Ladybug Tools utilize weather station wind data from EPW files, similar to the approach employed in this study, or the Butterfly plug-in, which employs CFD simulations utilizing the OpenFOAM framework. Ladybug Tools effectively models vegetation by simulating evapotranspiration, radiation exchanges, and thermal properties. However, these tools have limitations, as they treat vegetation properties as static, such as plant height and leaf area index (LAI). Furthermore, the potential impact of central area pollution on solar radiation magnitude was not considered in this study, as the weather data were obtained from the Turin-Caselle Airport station, which is situated in a rural environment.

6. Conclusion

This study underscores the considerable potential of VGSs, particularly green walls, in mitigating UHI effects and enhancing urban microclimates under both current and future climate scenarios. While the reductions in outdoor air temperature were modest, with variations ranging from -1.6°C to 1.3°C , the impact on T_{mrt} was more pronounced, with reductions reaching up to -2.27°C during peak solar radiation in summer periods. These improvements were most evident in urban canyons and areas with low SVF, thereby demonstrating the capacity of green walls to improve thermal comfort in densely populated urban environments. The UTCI also showed consistent improvements, with maximum reductions of 0.55°C under future climate projections for 2050 at noon in summer. Green walls proved particularly effective during summer, reducing cooling demand and lowering (cei) by up to 31%. However, during winter, a slight increase in heating demand led to higher emissions, underscoring the importance of optimizing green wall designs for seasonal energy performance. The findings indicate that the effectiveness of

green walls is contingent on factors such as building orientation, solar exposure, and local urban morphology. Ensuring sufficient sunlight for vegetation is imperative for sustaining growth and optimizing the cooling effects driven by evapotranspiration. In the context of projected climate change, green walls are poised to play a pivotal role in adapting urban environments to rising temperatures and increasingly frequent heat waves.

While the present study did not examine partial coverage, this is an intriguing area for future research. The optimization of the model to achieve comparable performance with reduced coverage ratios could significantly increase its practicality. Furthermore, advancements in this field could include the incorporation of locally adapted plant species, leveraging their distinctive thermal characteristics to enhance cooling efficiency, and adapting to diverse climatic and urban conditions.

In summary, the integration of green walls emerges as a pragmatic and sustainable approach to enhance outdoor thermal comfort, curtail carbon emissions, and mitigate Urban Heat Island (UHI) effects, particularly within urban contexts characterized by densely developed environments. These findings provide a solid foundation for integrating green walls into comprehensive urban climate adaptation strategies.

Note on Publication

This thesis has been adapted and expanded from the following published article: Dehghan Lotfabad, A., Hosseini, S. M., Dabove, P., Heiranipour, M., & Sommese, F. (2025). Impacts of Vertical Greenery on Outdoor Thermal Comfort and Carbon Emission Reduction at the Urban Scale in Turin, Italy. *Buildings*, 15(3), 450. <https://doi.org/10.3390/buildings15030450>

The article, published in the MDPI Buildings journal, presents the core findings and methodologies of this research. This thesis provides a more comprehensive exploration of the topic, including additional analysis, discussions, and extensions of the original work. Readers are encouraged to refer to the published article for further details on the initial study. The article can be accessed and downloaded via the following link:

<https://www.mdpi.com/2075-5309/15/3/450>

Acknowledgments:

We would like to acknowledge that this study is a part of our contribution within the framework of the “PNRR”: SPOKE 7 “CCAM, Connected Networks, and Smart Infrastructure”-WP4.

Abbreviations

The following abbreviations are used in this manuscript:

BT	Brightness Temperature	MWh	Megawatt Hour
cei	Carbon Emission Intensity	NDVI	Normalized Different Vegetation Index
CFD	Computational Fluid Dynamics	NIR	Near-infrared
CVRMSE	Cumulative Variation of Root Mean Squared Error	PET	Physiological Equivalent Temperature
EGR	Extensive Green Roof	SL	Street Length
ERF	Effective Radiant Field	SUHI	Surface Urban Heat Island
GWs	Green Wall	SVF	Sky View Factor
HS	Heavy Systems	TIR	Thermal Infrared
HVAC	Heating, Ventilation, and Air Conditioning	Tmrt	Mean Radiant Temperature
LAI	Leaf Area Index	TMY	Typical Meteorological Year
LS	Light Systems	UHI	Urban Heat Island
LST	Last Surface Temperature	UTCI	Universal Thermal Climate Index
MBE	Mean Bias Error	UWG	Urban Weather Generator
MV	Mur Vegetal	VGSs	Vertical Greenery Systems

Nomenclature

a_{lw}	Long wave absorptivity/emissivity (clothing) default 0.95	T_i	Surface temperature
A_p/AD	The projection factor is determined through a look-up table available at ASHRAE and is determined by solar altitude, solar azimuth, and the body's related angle.	AL	Band-Specific Additive Rescaling Factor
a_{sw}	Short wave absorptivity of the person (skin and clothing) default 0.7	C	Stephan-Boltzmann constant
f_{bes}	Fraction of body exposed to direct solar radiation	σ	Stefan Boltzmann constant (5.667×10^{-8})
f_{eff}	Fraction of the body that can radiate heat (related to posture)	H	Planck constant
f_{svv}	Sky view factor	H/W	Aspect ratio
h_r	Radiant heat transfer coefficient	LA	Total spectral radiance
I_{diff}	Diffuse radiation (W/m ²)	ML	Band-specific multiplicative rescaling factor
I_{dir}	Direct radiation (W/m ²)	Qcal	Band 10
I_{th}	Global horizontal radiation (W/m ²)	TOA	Total spectral radiance
R_{floor}	Ground reflectance	ε	Land surface emissivity
F_i	View factors to each surface	λ	Emitted radiance
P_v	Proportion of Vegetation	c	Light velocity
T_a	Dry bulb temperature	ε_{person}	The emissivity of the human (assumed to be 0.95)

Appendix A

Appendix A.1

High-precision meteorological data Table A1 was used to validate the simulation results, allowing for reliable comparisons between observed environmental conditions and model predictions.

Table A1. Insite measurements sensors characteristics.

Wind Vane Anemometer DV20	
Anodized aluminum weathervane/Long-life potentiometric transducer	
Measuring range	0° – 360°
Resolution	0.35° for the system
Precision	±2.8°
Operating temperature	0C – + 60 °C; -30 – +60 °C with electric heater
Dimensions	561 × 406(mm)
Weight	0.9 (kg)
Tachometer Anemometer Vv20	
Three-blade polycarbonate reel/solid-state measuring transducer with frequency output	
Safety field	0 – 220 (km/h), 61 (m/s)
Resolution	0.06 (m/s), 0.2 (km/h)
Sensitivity	less than 0.02 (m/s), threshold of 1.8 (km/h), 0.5 (m/s)
Precision	±0.25 (km/h), 0.07 (m/sec) or 1% of reading
Operating temperature	from -30 °C to +60 °C (with heater)
Dimensions	178 (Ø) × 281 (mm)
Weight	0.9 (kg)
Support Arm BSA20	
Made entirely of stainless steel / Comes complete with cables and connectors for sensors	
Dimensions	1490 × 790 (mm)
Weight	6.5 (kg) (including sensors)
Lightning rod made of stainless steel	1700 (mm) long/10 (mm) in diameter
Pyranometer HE20K	
Measuring range	0 – 1500 (W/m ²)
Spherical window	305 – 2800 (nm)
Non-linearity	±1.5% in the range 0 – 1000 (W/m ²)
Operating temperature range	-40 – +60 °C
Precision	5% (daily total), 1st class WMO (ISO 9060)
Influencing factors	sensitivity dependence on temperature < 2% in the range from -10 °C to +40 °C
Dimensions	150 (Ø) × 115 (mm)
Weight	1 (kg) (with shield)
THS Thermo-Hygrometer	
Hygrometer – Measurement range	0 to 100% RH
HYGROMETER – Temperature range	-50 – +100 °C
SHIELDED AIR THERMOMETER – Sensing element	PT100 1/3 Din Class A
HYGROMETER – Accuracy	±1.5% from 0 to 100% RH

SHIELDED AIR THERMOMETER—
Measurement range

–50 – +100 °C

SHIELDED AIR THERMOMETER—Ac-
curacy at 23 °C

±0.2 °C

PG10 and PG10R

Connection with Data-logger

Interface RS-485 with SDI-12 protocol

Measurement Range

up to 1000 (mm/h)

Output Resolution

0.1 (mm)

Collecting Area

1000 (cm²)

Accuracy

Max 3% < 800 (mm/h), Max 5%, 800 – 1000 (mm/h)

Temperature Range

PG10: 32 °F/140 °F, 0 °C/60 °C, PG10R: –22 °F/140 °F,
–30 °C/60 °C

Sensor Type

Tipping bucket rain gauge

Appendix B

Appendix B.1

Figure B1 compares the levels of direct solar radiation recorded in the EPW weather file under current conditions and future projections in 2050. It shows how the intensity and distribution of solar radiation change over time and provides valuable context for understanding future climate scenarios.

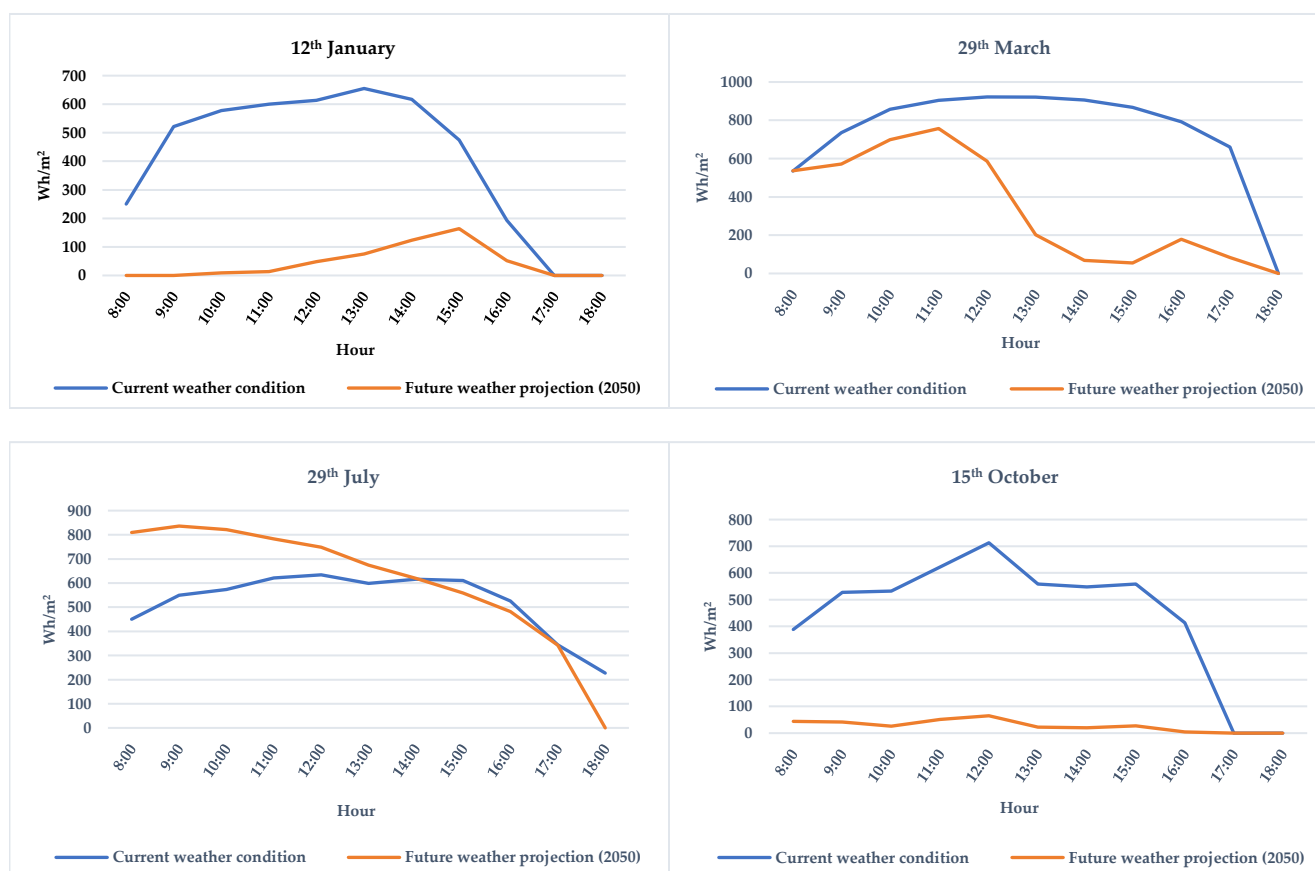


Figure B1. Direct solar radiation under current weather conditions and 2050 projection, based on data from the original EPW file.

Sources of Figures

The following figures in this thesis were created by the author and have been published in the article:

Dehghan Lotfabad, A., Hosseini, S. M., Dabove, P., Heiranipour, M., & Sommese, F. (2025). Impacts of Vertical Greenery on Outdoor Thermal Comfort and Carbon Emission Reduction at the Urban Scale in Turin, Italy. *Buildings*, 15(3), 450. <https://doi.org/10.3390/buildings15030450>

Figure 1: Drivers of urban heat islands and the scope of the study.

Figure 2: Flowchart of the analysis of the SUHI and site selection along with the simulation workflow.

References

1. United Nations, D. of E. and S.A.P.D. *World Urbanization Prospects: The 2014 Revision*; New York, 2015;
2. Ng, E.; Chen, L.; Wang, Y.; Yuan, C. A Study on the Cooling Effects of Greening in a High-Density City: An Experience from Hong Kong. *Build Environ* **2012**, 47, 256–271, doi:10.1016/j.buildenv.2011.07.014.
3. De Groeve, M.; Kale, E.; Godts, S.; Orr, S.A.; De Kock, T. Impact of Vertical Greening on Urban Microclimate and Historic Building Materials: A Meta-Analysis. *Build Environ* **2024**, 253, doi:10.1016/j.buildenv.2024.111365.
4. Boccalatte, A.; Fossa, M.; Thebault, M.; Ramousse, J.; Ménézo, C. Mapping the Urban Heat Island at the Territory Scale: An Unsupervised Learning Approach for Urban Planning Applied to the Canton of Geneva. *Sustain Cities Soc* **2023**, 96, 104677, doi:10.1016/j.scs.2023.104677.
5. Cheval, S.; Amihăesei, V.-A.; Chitu, Z.; Dumitrescu, A.; Falcescu, V.; Iraşoc, A.; Micu, D.M.; Mihuleţ, E.; Ontel, I.; Paraschiv, M.-G.; et al. A Systematic Review of Urban Heat Island and Heat Waves Research (1991–2022). *Clim Risk Manag* **2024**, 44, 100603, doi:10.1016/j.crm.2024.100603.
6. Schmidt, V. Urban Morphology as a Key Parameter for Mitigating Urban Heat? – A Literature Review. *IOP Conf Ser Earth Environ Sci* **2024**, 1363, 012074, doi:10.1088/1755-1315/1363/1/012074.
7. Zheng, Y.; Ren, C.; Shi, Y.; Yim, S.H.L.; Lai, D.Y.F.; Xu, Y.; Fang, C.; Li, W. Mapping the Spatial Distribution of Nocturnal Urban Heat Island Based on Local Climate Zone Framework. *Build Environ* **2023**, 234, 110197, doi:10.1016/j.buildenv.2023.110197.
8. Eslamirad, N.; Sepúlveda, A.; De Luca, F.; Sakari Lylykangas, K.; Ben Yahia, S. Outdoor Thermal Comfort Optimization in a Cold Climate to Mitigate the Level of Urban Heat Island in an Urban Area. *Energies (Basel)* **2023**, 16, 4546, doi:10.3390/en16124546.
9. Gholami, H.; Kamelnia, H.; Mahdavinejad, M.J.; Sangin, H. Optimizing Building Configuration and Orientation for Social Housing Projects in Iran. *Iranica Journal of Energy and Environment* **2025**, 16, 289–308, doi:10.5829/ijee.2025.16.02.11.

10. Rabie, S.; Sangin, H.; Zandieh, M. The Orientation of Village, the Most Important Factor in Rural Sustainability in Cold Climate (Case Study: Masuleh and Uramantakht). *Journal of Solar Energy Research* **2021**, *6*, 761–776, doi:10.22059/jser.2021.315862.1187.
11. Shao, L.; Liao, W.; Li, P.; Luo, M.; Xiong, X.; Liu, X. Drivers of Global Surface Urban Heat Islands: Surface Property, Climate Background, and 2D/3D Urban Morphologies. *Build Environ* **2023**, *242*, 110581, doi:10.1016/j.buildenv.2023.110581.
12. Lin, T.-P.; Matzarakis, A.; Hwang, R.-L. Shading Effect on Long-Term Outdoor Thermal Comfort. *Build Environ* **2010**, *45*, 213–221, doi:10.1016/j.buildenv.2009.06.002.
13. T.R.OKE *Boundary Layer Climates*; Routledge: London, UK, 2002; ISBN 0-203-71545-4.
14. Güller, C.; Toy, S. The Impacts of Urban Morphology on Urban Heat Islands in Housing Areas: The Case of Erzurum, Turkey. *Sustainability* **2024**, *16*, 791, doi:10.3390/su16020791.
15. Ahmadi Venhari, A.; Tenpierik, M.; Taleghani, M. The Role of Sky View Factor and Urban Street Greenery in Human Thermal Comfort and Heat Stress in a Desert Climate. *J Arid Environ* **2019**, *166*, 68–76, doi:10.1016/j.jaridenv.2019.04.009.
16. Fang, Z.; He, H.; Mao, Y.; Feng, X.; Zheng, Z.; Guo, Z. Investigating an Accurate Method for Measuring the Outdoor Mean Radiation Temperature. *International Journal of Thermal Sciences* **2023**, *188*, 108219, doi:10.1016/j.ijthermalsci.2023.108219.
17. Azimi, Z.; Shafaat, A. Proposing Design Strategies for Contemporary Courtyards Based on Thermal Comfort in Cold and Semi-Arid Climate Zones. *Build Environ* **2024**, *266*, 112150, doi:10.1016/j.buildenv.2024.112150.
18. Li, J.; Wang, J.; Wong, N.H. Urban Micro-Climate Research in High Density Cities: Case Study in Nanjing. *Procedia Eng* **2016**, *169*, 88–99, doi:10.1016/j.proeng.2016.10.011.
19. Irfeey, A.M.M.; Chau, H.-W.; Sumaiya, M.M.F.; Wai, C.Y.; Muttill, N.; Jamei, E. Sustainable Mitigation Strategies for Urban Heat Island Effects in Urban Areas. *Sustainability* **2023**, *15*, 10767, doi:10.3390/su151410767.
20. Lopez-Cabeza, V.P.; Alzate-Gaviria, S.; Diz-Mellado, E.; Rivera-Gomez, C.; Galan-Marin, C. Albedo Influence on the Microclimate and Thermal Comfort of Courtyards under Mediterranean Hot Summer Climate Conditions. *Sustain Cities Soc* **2022**, *81*, 103872, doi:10.1016/j.scs.2022.103872.
21. Morakinyo, T.E.; Lam, Y.F. Simulation Study on the Impact of Tree-Configuration, Planting Pattern and Wind Condition on Street-Canyon's Micro-Climate and Thermal Comfort. *Build Environ* **2016**, *103*, 262–275, doi:10.1016/j.buildenv.2016.04.025.
22. Cortês, A.S.B.; Almeida, J.A.S.; Kanoun-Boulé, M.; Tadeu, A. Green Facades and Living Walls: The Portuguese Experience. In *INCREEaSE*; Springer International Publishing: Cham, 2018; pp. 562–570 ISBN 978-3-319-70271-1.
23. Zaina, S.M.; Fadli, F.; Hosseini, S.M. Evaluation of Smart Irrigation Systems in Hot-Arid Climates for Green Roofs and Walls: Case of Doha, Qatar. *Smart and Sustainable Built Environment* **2022**, *11*, 346–367, doi:10.1108/SASBE-11-2021-0201.
24. Ramadhan, A.M.; Mahmoud, A.H. Evaluating the Efficiency of a Living Wall Facade as a Sustainable Energy-Saving Alternative in Hot Arid Regions. *Journal of Engineering and Applied Science* **2023**, *70*, 96, doi:10.1186/s44147-023-00259-9.
25. Reynolds, H.L.; Brandt, L.; Fischer, B.C.; Hardiman, B.S.; Moxley, D.J.; Sandweiss, E.; Speer, J.H.; Fei, S. Implications of Climate Change for Managing Urban Green

-
- Infrastructure: An Indiana, US Case Study. *Clim Change* **2020**, 163, 1967–1984, doi:10.1007/s10584-019-02617-0.
26. Sommesse, F. Nature-Based Solutions to Enhance Urban Resilience in the Climate Change and Post-Pandemic Era: A Taxonomy for the Built Environment. *Buildings* **2024**, 14, 2190, doi:10.3390/buildings14072190.
 27. Susca, T.; Zanghirella, F.; Del Fatto, V. Building Integrated Vegetation Effect on Micro-Climate Conditions for Urban Heat Island Adaptation. Lesson Learned from Turin and Rome Case Studies. *Energy Build* **2023**, 295, 113233, doi:10.1016/j.enbuild.2023.113233.
 28. Wang, P.; Wong, Y.H.; Tan, C.Y.; Li, S.; Chong, W.T. Vertical Greening Systems: Technological Benefits, Progresses and Prospects. *Sustainability* **2022**, 14, 12997, doi:10.3390/su142012997.
 29. Zhang, L.; Deng, Z.; Liang, L.; Zhang, Y.; Meng, Q.; Wang, J.; Santamouris, M. Thermal Behavior of a Vertical Green Facade and Its Impact on the Indoor and Outdoor Thermal Environment. *Energy Build* **2019**, 204, 109502, doi:10.1016/j.enbuild.2019.109502.
 30. Larsen, S.F.; Filippín, C.; Lesino, G. Thermal Simulation of a Double Skin Façade with Plants. *Energy Procedia* **2014**, 57, 1763–1772, doi:10.1016/j.egypro.2014.10.165.
 31. Herath, H.M.P.I.K.; Halwatura, R.U.; Jayasinghe, G.Y. Modeling a Tropical Urban Context with Green Walls and Green Roofs as an Urban Heat Island Adaptation Strategy. *Procedia Eng* **2018**, 212, 691–698, doi:10.1016/j.proeng.2018.01.089.
 32. Mutani, G.; Todeschi, V. The Effects of Green Roofs on Outdoor Thermal Comfort, Urban Heat Island Mitigation and Energy Savings. *Atmosphere (Basel)* **2020**, 11, 123, doi:10.3390/atmos11020123.
 33. Ciacci, C.; Banti, N.; Di Naso, V.; Bazzocchi, F. Green Strategies for Improving Urban Microclimate and Air Quality: A Case Study of an Italian Industrial District and Facility. *Build Environ* **2023**, 244, 110762, doi:10.1016/j.buildenv.2023.110762.
 34. Kim, E.S.; Yun, S.H.; Lee, D.K.; Kim, N.Y.; Piao, Z.G.; Kim, S.H.; Park, S. Quantifying Outdoor Cooling Effects of Vertical Greening System on Mean Radiant Temperature. *Developments in the Built Environment* **2023**, 15, 100211, doi:10.1016/j.dibe.2023.100211.
 35. Djedjig, R.; Belarbi, R.; Bozonnet, E. Green Wall Impacts inside and Outside Buildings: Experimental Study. *Energy Procedia* **2017**, 139, 578–583, doi:10.1016/j.egypro.2017.11.256.
 36. Zuckerman, N.; Shiloah, N.; Lensky, I.M. Quantifying the Impact of Vertical Greenery Systems (VGS) on Mediterranean Urban Microclimate during Heat Wave Events. *Build Environ* **2025**, 267, 112151, doi:10.1016/j.buildenv.2024.112151.
 37. Taher, H.; Elsharkawy, H.; Rashed, H.F. Urban Green Systems for Improving Pedestrian Thermal Comfort and Walkability in Future Climate Scenarios in London. *Buildings* **2024**, 14, 651, doi:10.3390/buildings14030651.
 38. Nashaat, B. Optimizing Parametric Green Facades for Daylighting and Thermal Comfort in Egypt's Hot Climates. *Port-Said Engineering Research Journal* **2024**, 0, 0–0, doi:10.21608/pserj.2024.307043.1354.
 39. Wahba, S.; Kamil, B.; Nassar, K.; Abdelsalam, A. Green Envelop Impact on Reducing Air Temperature and Enhancing Outdoor Thermal Comfort in Arid Climates. *Civil Engineering Journal* **2019**, 5, 1124–1135, doi:10.28991/cej-2019-03091317.

40. U.S.G. Survey Available online: <https://earthexplorer.usgs.gov/> (accessed on 2 February 2025).
41. Ladybug Tools EPW Map Available online: <https://www.ladybug.tools/epwmap/> (accessed on 8 March 2024).
42. Agenzia Regionale per la Protezione Ambientale (ARPA) Piemonte di Torino Hourly Meteorological and Hydrological Data Available online: <https://www.arpa.piemonte.it/> (accessed on 2 May 2024).
43. Machard, A.; Salvati, A.; P. Tootkaboni, M.; Gaur, A.; Zou, J.; Wang, L.L.; Baba, F.; Ge, H.; Bre, F.; Bozonnet, E.; et al. Typical and Extreme Weather Datasets for Studying the Resilience of Buildings to Climate Change and Heatwaves. *Sci Data* **2024**, *11*, 531, doi:10.1038/s41597-024-03319-8.
44. Heiranipour, M.; Favoino, F.; Juaristi Gutierrez, M.; Avesani, S. *Typical and Extreme (Heatwave) Future Weather for Building Energy Simulations: Case for Turin and Bolzano, Italy, and De Bilt, Netherlands*; Zenodo: Genève, Switzerland, 2024;
45. Boccardo, P.; Giulio Tonolo, F. Remote Sensing Role in Emergency Mapping for Disaster Response. In *Engineering Geology for Society and Territory - Volume 5*; Springer International Publishing: Cham, 2015; pp. 17–24.
46. Avdan, U.; Jovanovska, G. Algorithm for Automated Mapping of Land Surface Temperature Using LANDSAT 8 Satellite Data. *J Sens* **2016**, *2016*, 1–8, doi:10.1155/2016/1480307.
47. Kasniza Jumari, N.A.S.; Ahmed, A.N.; Huang, Y.F.; Ng, J.L.; Koo, C.H.; Chong, K.L.; Sherif, M.; Elshafie, A. Analysis of Urban Heat Islands with Landsat Satellite Images and GIS in Kuala Lumpur Metropolitan City. *Heliyon* **2023**, *9*, e18424, doi:10.1016/j.heliyon.2023.e18424.
48. Rahman, Md.N.; Rony, Md.R.H.; Jannat, F.A.; Chandra Pal, S.; Islam, Md.S.; Alam, E.; Islam, A.R.Md.T. Impact of Urbanization on Urban Heat Island Intensity in Major Districts of Bangladesh Using Remote Sensing and Geo-Spatial Tools. *Climate* **2022**, *10*, 3, doi:10.3390/cli10010003.
49. Dabove, P.; Daud, M.; Olivotto, L. Revolutionizing Urban Mapping: Deep Learning and Data Fusion Strategies for Accurate Building Footprint Segmentation. *Sci Rep* **2024**, *14*, 13510, doi:10.1038/s41598-024-64231-0.
50. Regione Piemonte Geo Piemonte Available online: <https://geoportale.igr.piemonte.it/cms/> (accessed on 31 March 2024).
51. Rezaei, F.; Sangin, H.; Heiranipour, M.; Attia, S. A Multi-Objective Optimization of Window and Light Shelf Design in Office Buildings to Improve Occupants' Thermal and Visual Comfort. *Journal of Daylighting* **2024**, *11*, 55–68, doi:10.15627/jd.2024.4.
52. Naboni, E.; Milella, A.; Vadalà, R.; Fiorito, F. On the Localised Climate Change Mitigation Potential of Building Facades. *Energy Build* **2020**, *224*, 110284, doi:10.1016/j.enbuild.2020.110284.
53. Mackey, C.; Galanos, T.; Norford, L.; Sadeghipour Roudsari, M. Wind, Sun, Surface Temperature, and Heat Island: Critical Variables for High-Resolution Outdoor Thermal Comfort. In *Proceedings of the Proceedings of Building Simulation 2017: 15th Conference of IBPSA*; IBPSA: San Francisco, USA, August 7 2017; pp. 985–993.

54. Salvati, A.; Kolokotroni, M. Urban Microclimate and Climate Change Impact on the Thermal Performance and Ventilation of Multi-Family Residential Buildings. *Energy Build* **2023**, *294*, 113224, doi:10.1016/j.enbuild.2023.113224.
55. Dardir, M.; Berardi, U. Development of Microclimate Modeling for Enhancing Neighborhood Thermal Performance through Urban Greenery Cover. *Energy Build* **2021**, *252*, 111428, doi:10.1016/j.enbuild.2021.111428.
56. naboni, emanuele; meloni, marco; makey, chris; kaempf, jerome The Simulation of Mean Radiant Temperature in Outdoor Conditions: A Review of Software Tools Capabilities.; 2019; pp. 3234–3241.
57. Bueno, B.; Norford, L.; Hidalgo, J.; Pigeon, G. Prediction of the Urban Heat Island Effect to Be Used in Building Energy Analyses. In Proceedings of the Proceedings of SimBuild Conference 2012: 5th conference of IBPSA USA; IBPSA USA: Madison, USA, August 2012; Vol. 5, pp. 236–245.
58. Arens, E.; Hoyt, T.; Zhou, X.; Huang, L.; Zhang, H.; Schiavon, S. Modeling the Comfort Effects of Short-Wave Solar Radiation Indoors. *Build Environ* **2015**, *88*, 3–9, doi:10.1016/j.buildenv.2014.09.004.
59. American Society of Heating Georgia), R. and A.C.E. (Atlanta *Ashrae Guideline 14-2014: Measurement of Energy, Demand and Water Savings*; ASHRAE guideline; American Society of Heating, Refrigerating, and Air-Conditioning Engineers, 2014;
60. (NREL), N.R.E.L. EnergyPlus™ 2017.
61. Arenghi, A.; Perra, C.; Caffi, M. Simulating and Comparing Different Vertical Greenery Systems Grouped into Categories Using EnergyPlus. *Applied Sciences* **2021**, *11*, 4802, doi:10.3390/app11114802.
62. Hosseini, S.M.; Heiranipour, M.; Wang, J.; Hinkle, L.E.; Triantafyllidis, G.; Attia, S. Enhancing Visual Comfort and Energy Efficiency in Office Lighting Using Parametric-Generative Design Approach for Interactive Kinetic Louvers. *Journal of Daylighting* **2024**, *11*, 69–96, doi:10.15627/jd.2024.5.
63. Stec, W.J.; Paassen, A.H.C. van Symbiosis of the Double Skin Façade with the HVAC System. *Energy Build* **2005**, *37*, 461–469, doi:10.1016/j.enbuild.2004.08.007.
64. The International Energy Agency (IEA) Greenhouse Gas Emissions from Energy Data Explorer Available online: <https://www.iea.org> (accessed on 16 December 2024).